Modeling in the Neurosciences
From Biological Systems to Neuromimetic Robotics

Second Edition

Edited by
G.N. Reeke, R.R. Poznanski, K.A. Lindsay, J.R. Rosenberg and O. Sporns

Taylor & Francis, 2005
Boca Raton, Florida, USA

Chapter 5
pp. 89 - 115
(Preprint)

NATURAL VARIABILITY IN THE GEOMETRY OF DENDRITIC BRANCHING PATTERNS

Jaap van Pelt and Harry B.M. Uylings

Graduate School Neurosciences Amsterdam
Netherlands Institute for Brain Research
Meibergdreef 33, 1105 AZ Amsterdam
The Netherlands

Correspondence to:
Dr. Jaap van Pelt
Netherlands Institute for Brain Research
Meibergdreef 33
1105 AZ Amsterdam
Phone: (31) 20 5665481
Fax: (31) 20 6961006
E-mail: j.van.pelt@nih.knaw.nl

1. INTRODUCTION

Dendritic branching patterns are complex and show a large degree of variation in their shapes, within as well as between different cell types and species. This variation is found in typical shape parameters, such as the number, length and connectivity pattern (topological structure) of the segments in the dendritic tree, the curved nature of these segments and the embedding of the dendrite in three-dimensional (3D) space (Uylings and Van Pelt, 2002). Dendritic structure plays an important role in the spatial and temporal integration of postsynaptic potentials, both metrically (e.g., Rall et al., 1992; Rapp et al., 1994) and topologically (Van Pelt and Schierwagen, 1994, 1995; Van Ooyen et al., 2002), and is consequently an important determinant for the characteristics of neuronal firing patterns (e.g., Mason and Larkman, 1990; Mainen and Sejnowski, 1996; Sheasby and Fohlmeister, 1999; Washington et al., 2000; Bastian and Nguyenkim, 2001, Schaefer et al., 2003). A good account of the extent of dendritic morphological variation between individual dendritic trees is needed in order to explore its implications for neuronal signal integration. Dendritic morphological variation can be expressed by means of distribution functions for specific shape parameters, but functional properties need to be determined for complete dendritic trees. When original reconstructions are not available in sufficient number, one may use representative dendrites, synthesized using models of dendritic structures.

Among the algorithmic approaches to synthesize dendritic trees with geometrical characteristics and variation similar to those of observed dendrites two different classes can roughly be distinguished. In the *reconstruction model approach* dendritic shapes are reconstructed using empirical distribution functions for the shape parameters. Representative dendrites are obtained by random sampling of these distributions. For instance, Burke et al. (1992) used empirically obtained distribution functions for the length and diameters of dendritic branches and for the diameter relations at bifurcation points. Random dendrites were generated by a repeated process of random sampling of these distributions for deciding whether an elongating neurite should branch and for obtaining the diameters of the daughter branches. The modeled dendrites obtained in this way conform to the original distribution functions for shape characteristics. These algorithms are further elaborated and extended to include orientation in 3D space and incorporating environmental influences (Ascoli et al., 2001; Ascoli 2002a,b). An important assumption in this approach is that the shape parameters are independent from each other. Kliemann (1987) considered the segments at a given centrifugal order as individuals of a generation, which may give rise to individuals in a next generation (i.e., by producing a bifurcation point with two daughter segments). Mathematically, such a dendritic reconstruction could be described by a Galton-Watson process, based on empirically obtained splitting probabilities for defining per generation whether or not a segment will be a terminal or an intermediate one. Also in this example it is assumed that the successive choices in the reconstruction of a dendrite are independent. The model's predictability of branching patterns was greatly enhanced by including a systematic component additional to the random one (Carriquiry et al., 1991). Applications of this method to dendritic growth *in vitro* can be found in Uemura et al. (1995). Tamori (1993) used a set of six 'fundamental parameters' to describe dendritic morphology, and introduced a principle of least effective volume to derive dendritic branch angles.

In contrast to the reconstruction model approach, the *growth model approach* is based on modeling dendritic structure from principles of dendritic development. Neurons grow out by a process of elongation and branching of their neuritic extensions. These processes are governed by the dynamic behavior of growth cones, highly motile structures at the tips of outgrowing neurites. Neurite elongation requires the polymerization of tubulin into cytoskeletal microtubules. Branching occurs when a growth cone, including its actin cytoskeletal meshwork, splits in two parts while partitioning the number of microtubules, and each daughter growth cone continuing to grow on their own (e.g., Black (1994); Kater et al., (1994); Kater and Rehder, (1995); Letourneau et al.,

(1994). Growth cones may also retract by microtubule depolymerization, or may redirect their orientations. The dynamic behavior of a growth cone results from the integrated outcome of many intracellular mechanisms and interactions with its local environment. These include, for instance, the exploratory interactions of filopodia with a variety of extracellular (e.g., guidance, chemorepellant, chemoattractant) molecules in the local environment (e.g. Kater et al., 1994, McAllister, 2002; Whitford et al., 2002), receptor mediated trans-membrane signaling to cytoplasmic regulatory systems (e.g. Letourneau et al., 1994), intracellular regulatory genetic and molecular signaling pathways (e.g., Song and Poo, 2001), and electrical activity (e.g., Cline, 1999; Ramakers et al., 1998, 2001; Zhang and Poo, 2001). Especially electrical activity and neurotransmitters have a strong modulatory influence on neurite outgrowth via their effects on intracellular calcium levels and on gene expression, by which many different proteins are being involved, such as neuroptrophins, GAP43, CaMKII and CPG15 (reviewed in Cline, 1999). Further regulatory influences are exerted by the phosphorylation state of microtubule associated proteins (MAPs) on the stabilization of the microtubule cytoskeleton (modeled in Van Ooyen and Van Pelt, 2002). There is increasing evidence that the Rho family of small GTPases, including Rho, Rac and Cdc42 play an important role in neuronal development. These molecules act as molecular switches in signaling pathways down to the actin cytoskeleton within the growth cone. Their role in neuronal development is further stressed by the fact that mutations in their genes are especially involved in the origin of mental retardation, suggesting the development of abnormal neuronal network structures (Ramakers, 2002).

In addition to these regulatory mechanisms, the dendritic outgrowth process may also be subjected to basic constraints, which limit their modulatory responsiveness. For instance, neurite elongation proceeds by growing mitrotubules, which requires the production, transport and polymerization of tubulin cytoskeletal elements. The production rate of cytoskeletal elements will set an upper limit to the averaged total length increase of the dendrite. In addition, the division of flow of cytoskeletal elements at a bifurcation will modulate the elongation rate of the daughter branches. Earlier model studies of microtubule polymerization (neurite elongation) in relation to tubulin production and transport demonstrated how limited supply conditions may lead to competition between growth cones for tubulin, resulting in alternating advance and immobilization (Van Ooyen et al, 2001). Empirical evidence for such competitive behavior has subsequently been obtained from time-lapse studies of outgrowing neurons in tissue culture by Ramakers (see Costa et al., 2002). Limiting resources may also lead to competitive phenomena between axons, where target derived neurotrophins are required for the maintenance and stabilization of synaptic axonal endings on target dendrites. Modeling studies have shown that the precise manner in which neurotrophins regulate the growth of axons determines what patterns of target innervation can develop (Van Ooyen and Willshaw, 1999). Taking a spatial dimension into account these authors show that the distance between axonal endings on the target dendritic tree mitigates competition and permits the coexistence of axons (Van Ooyen and Willshaw, 2000). These examples just illustrate the complexity of the outgrowth process in terms of involved molecules, interactions, signaling pathways and constraints. The integrated action and the details of all these intracellular and extracellular mechanisms will finally form the basis of dendritic morphological characteristics, of morphological differentiation between cell types and the diversity between neurons of the same type (e.g., Acebus and Ferrus, 2000).

Modeling neurite outgrowth at the level of the mentioned details is an immense task, being only in its early phase and proceeding in a step by step fashion by focusing on well manageable subsystems, such as the examples have shown. A phenomenological approach in modeling dendritic outgrowth, on the contrary, aims at finding the algorithmic framework to describe the behavior of growth cones directly in terms of elongation and branching rates. This approach is very powerful to obtain understanding of how dendritic shape characteristics and variations arise from the details in the elongation and branching rates. Because of the large number of processes involved

in the actual behavior of growth cones it is a reasonable assumption to model elongation and branching as outcomes of a stochastic process. Although the probability functions underlying this process may be very complex, it is an interesting question which minimal assumptions are required to obtain model dendrites, that compare closely in their morphological properties and variation to the observed ones. Experimental longitudinal studies on dendritic development in vivo are experimentally difficult to perform, because the tissue needs to be processed in order to enable morphological quantification. Tissue culture studies might form an alternative, although, especially in dissociated cultures, neurons develop in an environment, different from their natural one.

The *growth model approach* has been applied in the past decades by several investigators (e.g., Smit et al., 1972; Berry and Bradley, 1976; Van Pelt and Verwer, 1983, Ireland et al., 1985, Horsfield et al., 1987 and Nowakowski et al., 1992). One of the growth model approaches will be described in more detail in this chapter. It is based on the assumption that the growth actions are outcomes of a stochastic process. The branching and elongation probabilities allow a direct interpretation in terms of the underlying developmental biological process. Additionally, the dependence of these probabilities on developmental time and on the growing structure itself, are implicitly accounted for. It will be shown that the assumptions of random branching and random elongation of terminal segments (or 'growth cones') are sufficient for generating dendrites with realistic variations in the topological and metrical shape parameters. Because of the structure of the model the variables are directly related to the dynamic behavior of growth cones, which allows for empirical verification. This makes the model also of importance for developmental studies because it provides a tool for analyzing reconstructed dendrites in terms of 'hypothesized' developmental histories, which themselves are often not accessible by empirical techniques.

In the following sections, dendritic shape parameters are introduced and examples are given for the extent of their variations as found in observed dendritic trees. The dendritic growth model is reviewed and discussed, hereby following the modular extensions that have been incorporated in the course of time. The functional implications of dendritic morphological variation are briefly discussed.

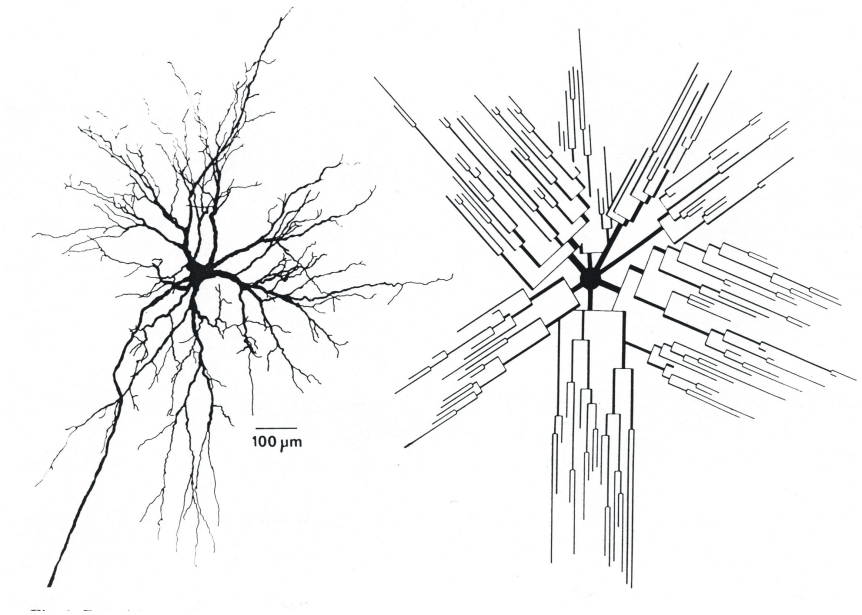

Figure 1. Left: Plane reconstruction of the soma-dendritic profile of a tecto-reticulo-spinal neuron of cat superior colliculus. Right: Approximation of neuronal arborizations by regular geometric bodies (reproduced from Schierwagen (1986) with permission of Schierwagen and the *J. Hirnforsch.*)

2. DENDRITIC SHAPE PARAMETERS

For the characterization of their shapes dendrites are generally simplified to regular geometric structures, which allow easy quantification. An example of such a simplification is given in Figure 1 for a cat superior colliculus neuron, in which the segments in the dendrites are stretched and represented by cylinders with a given length and diameter (Schierwagen, 1986).
The embedding in 3D-space and irregularity and curvature of the branches is hereby lost. The simplified dendrite is subsequently characterized by the number, length, diameter and connectivity pattern (*topological structure* or *tree type*) of its segments, i.e., the branches between successive bifurcation points and/or terminal tips. *Intermediate segments* (ending in a bifurcation point) and *terminal segments* are distinguished (Figure 2). A given segment can be labeled by its *degree* (denoting the number of terminal segments in its subtree) and/or by its *centrifugal order* (denoting the number of bifurcation points on the path from the root up to the segment). Bifurcation points are labeled by their *partitions*, i.e., the *degrees* of the two subtrees arising from that bifurcation. Dendritic morphological variation is expressed in terms of variations in these shape parameters.
Dendritic shape parameters have earlier been reviewed by Uylings et al. (1989), Verwer et al. (1992) and Uylings and Van Pelt (2002).

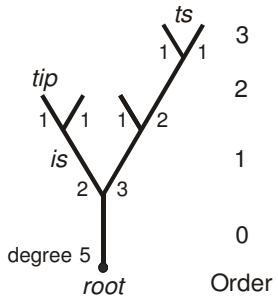

Figure 2. Elements of a topological tree, with a distinction of intermediate (*is*) and terminal (*ts*) segments. Segments are labeled according to the number of tips in their subtrees (*degree*) or distance from the root (*centrifugal order*).

2.1 Dendritic topology

2.1.1 *Connectivity pattern*

Topological variation arises because of the finite number of *tree types* that are possible for a given number of segments. A summary of all different tree types with up to and including 8 terminal segments is given in Figure 3 (taken from Van Pelt and Verwer, 1983). The trees are labeled by a rank number according to the ranking scheme described in Van Pelt and Verwer (1983). For 3D trees there is no distinction between left and right side at bifurcation points. Therefore, the trees could be displayed in a standardized way, such that at each bifurcation point the subtree with the highest rank number is drawn at the right side. The number of 3D-tree types with n terminal segments, N_α^n, (α denoting the set of 3D-tree types) is given by the iterative equation

$$N_\alpha^n = \frac{1}{2}\left(\sum_{r=1}^{n-1} N_\alpha^r N_\alpha^{n-r} + (1-\varepsilon(n)) N_\alpha^{n/2} \right) \quad \text{and} \quad N_\alpha^1 = 1 \tag{1}$$

(Harding, 1971), with $\varepsilon(n) = 0$ for even n and $\varepsilon(n) = 1$ for odd n. (2)

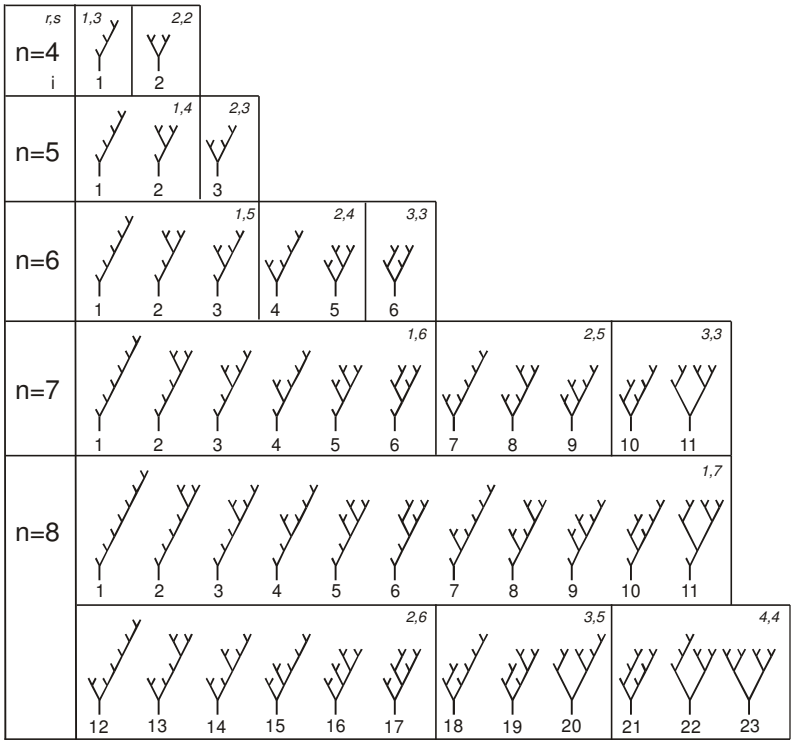

Figure 3. Table of tree types of degree n = 4-8. The trees are numbered according to a ranking scheme described in Van Pelt and Verwer (1983). The number pairs (*r,s*) above groups of tree types indicate the *degrees* of the first-order subtrees. The tree types are plotted in a standardized way with at a bifurcation the subtree with the highest rank number plotted to the right side.

The number of tree types increases rapidly with n and a reasonable approximation for the order of magnitude is given by $N_{\alpha}^{n} \approx 2.4^{n}$ (Van Pelt et al., 1992). [Note, that for 2D branching patterns, like rivers, the left-right distinction is meaningful and results in a larger number of 2D-tree types N_{τ}^{n} (with τ denoting the set of 2D tree-types) which relates to the number of terminal segments n by

$$N_{\tau}^{n} = \frac{1}{2n-1} \cdot \binom{2n-1}{n} \qquad (3)$$

(Caley, 1859; cf Shreve, 1966)].

2.1.2. *Tree asymmetry*

Tree-type frequency distributions become unmanageable large with larger n. A numerical index for the topological structure of a tree would therefore greatly facilitate the quantitative analysis of topological variation within a set of dendritic trees. Among the used topological indices, the *tree asymmetry index*, A_t, has proven to be the most discriminative one, i.e., being able to distinguish most (but not all) of the possible tree types (Van Pelt et al., 1989). The tree-asymmetry index A_t of a given tree α^{n} with n terminal segments (and thus with *n-1* bifurcation points) is defined by

$$A_t(\alpha^n) = \frac{1}{n-1}\sum_{j=1}^{n-1} A_p(r_j, s_j), \tag{4}$$

being the mean value of all the *n-1* partition asymmetries $A_p(r_j, s_j)$ in the tree, which, at each of the *n-1* bifurcation points, indicate the relative difference in the number of bifurcation points $r_j - 1$ and $s_j - 1$ in the two subtrees emerging from the j_{th} bifurcation point. The partition asymmetry A_p at a bifurcation is defined as

$$A_p(r, s) = \frac{|r - s|}{r + s - 2} \tag{5}$$

for $r + s > 2$, with r and s denoting the number of terminal segments in the two subtrees. $A_p(1,1) = 0$ by definition. The discrete values of the tree asymmetry index for trees up to and including *degree* 8 are shown in Figure 4.

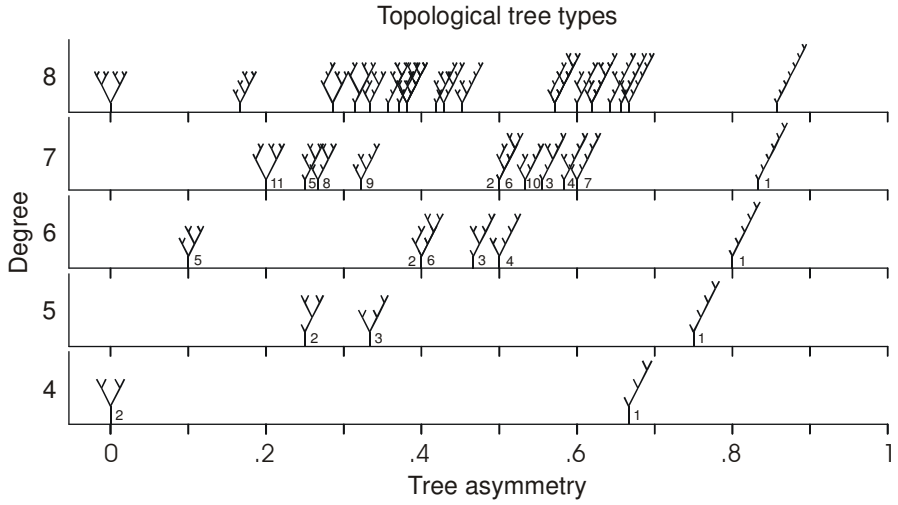

Figure 4. Tree-types of degree 4-8, plotted versus their tree-asymmetry value. The asymmetry values range from zero for fully symmetric trees (only possible when the degree is a power of two) to a maximum value for fully asymmetric trees, which value approaches one when the asymmetric tree becomes larger. The tree numbers correspond to those in Figure 2. Some trees have equal values for the asymmetry index and are plotted at the same position, for instance tree numbers 2 and 6 of degree 6.

Two different coding schemes are used to represent a topological tree by a linear string, i.e., the *label array* and the *branching code*. The *label array* representation is based on a standardized procedure to trace a tree along its bifurcation points and terminal tips, labeled by 1's and 0's, respectively. The tree is uniquely represented by the sequence of labels (see also Overdijk et al., 1978), which starts at the root segment and, at bifurcations, first follows the segment at the right side, while a label '1' is used for an intermediate segment and a label '0' for a terminal segment. For instance, tree number 11 of *degree* 7 in Figure 3 is represented by the array 1110010011000. For a tree of *degree n* the number of labels equals *2n-1* with *n-1* '1's and *n* '0's. Many of the $\binom{2n-1}{n}$ different permutations of such number of labels do not represent a tree. Actually, from each subset of permutations, which transform into each other by rotation, thus containing *2n-1* permutations,

only one of them represents a tree. This makes the total number of different (2D) tree types of degree n equal to $\binom{2n-1}{n}/(2n-1)$, which explains Equation 3. The *branching code* representation of a tree indicates iteratively at each bifurcation the number of terminal segments in both subtrees within brackets. The code starts with the number of terminal segments in the complete tree. For instance, the mentioned tree in Figure 3 is represented by the branching code 7(3(1 2(1 1)) 4(2(1 1) 2(1 1))). The *label arrays* and *branching codes* of the tree types with up to and including 8 terminal segments are given in Table 1. Note, that the used ranking scheme (see also Van Pelt and Verwer, 1983) is based on recurrency in the succession of trees. For instance, the sequence of trees of *degree* 6 is repeated as first-order subtrees in trees of *degree* 7.

Table 1. List of *label arrays*, *branching codes* and *tree-asymmetry* values of tree types with up to and including 8 terminal segments. Trees of equal degree are given a rank number as displayed in the 2nd column (see also Figure 3). The asymmetry index has been introduced by Van Pelt et al. (1992) and the given values are calculated according to option 1 for the asymmetry index definition in that paper (the values given by Uylings et al. (1989) have been calculated using option 2 and thus differ from the values listed below). Note, that the branching code of (sub)trees of *degree* 2 and 3 are expanded in the first two trees only.

Degree	No	Label array	Branching code	Asymmetry index
1	1	0	1	0
2	1	100	2(1 1)	0
3	1	11000	3(1 2(1 1))	0.500
4	1	1110000	4(1 3)	0.667
	2	1100100	4(2 2)	0
5	1	111100000	5(1 4(1 3))	0.750
	2	111001000	5(1 4(2 2))	0.250
	3	111000100	5(2 3)	0.333
6	1	11111000000	6(1 5(1 4(1 3)))	0.800
	2	11110010000	6(1 5(1 4(2 2)))	0.400
	3	11110001000	6(1 5(2 3))	0.467
	4	11110000100	6(2 4(1 3))	0.500
	5	11100100100	6(2 4(2 2))	0.100
	6	11100011000	6(3 3)	0.400
7	1	1111110000000	7(1 6(1 5(1 4(1 3))))	0.833
	2	1111100100000	7(1 6(1 5(1 4(2 2))))	0.500
	3	1111100010000	7(1 6(1 5(2 3)))	0.556
	4	1111100001000	7(1 6(2 4(1 3)))	0.583
	5	1111001001000	7(1 6(2 4(2 2)))	0.250
	6	1111000110000	7(1 6(3 3))	0.500
	7	1111100000100	7(2 5(1 4(1 3)))	0.600
	8	1111001000100	7(2 5(1 4(2 2)))	0.267
	9	1111000100100	7(2 5(2 3))	0.322
	10	1111000011000	7(3 4(1 3))	0.533
	11	1110010011000	7(3 4(2 2))	0.200
8	1	111111100000000	8(1 7(1 6(1 5(1 4(1 3)))))	0.857
	2	111111001000000	8(1 7(1 6(1 5(1 4(2 2)))))	0.571
	3	111111000100000	8(1 7(1 6(1 5(2 3))))	0.619
	4	111111000010000	8(1 7(1 6(2 4(1 3))))	0.643
	5	111110010010000	8(1 7(1 6(2 4(2 2))))	0.357

6	111110001100000	8(1 7(1 6(3 3)))	0.571
7	111111000001000	8(1 7(2 5(1 4(1 3))))	0.657
8	111110010001000	8(1 7(2 5(1 4(2 2))))	0.371
9	111110001001000	8(1 7(2 5(2 3)))	0.419
10	111110000110000	8(1 7(3 4(1 3)))	0.600
11	111100100110000	8(1 7(3 4(2 2)))	0.314
12	111111000000100	8(2 6(1 5(1 4(1 3))))	0.667
13	111110010000100	8(2 6(1 5(1 4(2 2))))	0.381
14	111110001000100	8(2 6(1 5(2 3)))	0.429
15	111110000100100	8(2 6(2 4(1 3)))	0.452
16	111100100100100	8(2 6(2 4(2 2)))	0.167
17	111100011000100	8(2 6(3 3))	0.381
18	111110000011000	8(3 5(1 4(1 3)))	0.619
19	111100100011000	8(3 5(1 4(2 2)))	0.333
20	111100010011000	8(3 5(2 3))	0.381
21	111100001110000	8(4(1 3) 4(1 3))	0.571
22	111001001110000	8(4(1 3) 4(2 2))	0.286
23	111001001100100	8(4(2 2) 4(2 2))	0

2.2 Dendritic metrics

The quantification of the metrical properties of dendritic trees (e.g., Uylings and Van Pelt, 2002) depends on the way of reconstruction. With present manual reconstruction techniques, the branches in the dendrite are approximated by one or more straight lines or cylinders. The metrical properties of such simplified dendritic tree are then determined by the length and diameter of its segments. Pathlengths are defined by the summed length of the segments between two characteristic points, like for instance between the root point and a terminal tip. The radial distance between two points in the original structure is determined by the length of the straight connecting line. The difference between pathlength and radial distance is an indication for the irregularity and curvature of the branches in the original dendritic structure. New reconstruction techniques, which are now under development, are based on digitized images of dendrites, for instance obtained via confocal microscopy. The digitized representations allow the use of powerful image analysis and differential geometry techniques to quantify (automatically) dendritic shape with a much more powerful repertoire of 3D shape descriptors, including multi scale fractal approaches (e.g., Costa et al., 2002, Streekstra and Van Pelt, 2002). Recent reviews of reconstruction approaches can be found in Jaeger (2000), Van Pelt et al., (2001c), and Ascoli (2002a).

2.2.1 *Segment length and diameter*

In the conventional manual reconstruction approach curved dendritic branches are approximated by a series of straight segments, with a given length and diameter. Dendritic segments, however, may be covered with spines, making the diameter an ill-defined quantity. Even in the case of smooth dendrites, the diameter may not be constant along the segment. One speaks of tapering if the diameter gradually decreases. Practically, in the case of irregularities the diameter is taken as an averaged value over several measuring points.

3. OBSERVED VARIABILITY IN DENDRITIC SHAPE PARAMETERS

3.1 Variation in topological structure

The topological variation in a set of dendrites is expressed by the frequencies of the different tree types. Such an outcome is given in Figure 5 for basal dendrites of rat cortical pyramidal cells (Uylings et al., 1990). Each panel displays the tree-type frequencies for a subgroup with a given number of terminal segments. The frequency distributions appear to be highly non-uniform, with some tree types abundantly present while others hardly occur. Especially for larger trees many possible tree types will not occur in a data set resulting in tree-type frequency distributions with many empty classes.

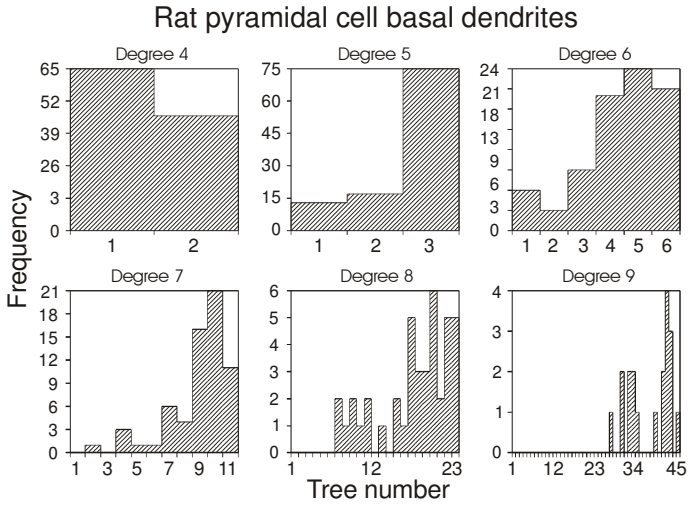

Figure 5. Frequency distributions of tree types observed in a set of basal dendrites of rat cortical pyramidal neurons. The tree numbers correspond to those in Figure 3. Note, that the distributions are highly non-uniform.

Rather than dealing with distributions of tree numbers, topological variation can also be expressed by the mean and standard deviation of the tree-asymmetry index. Examples of observed values for dendrites of different cell types are given in Table 2. These data show that both rat and guinea pig Purkinje cells have highest asymmetry values of about 0.5 with a small standard deviation because of the large number of bifurcations (partitions) in the trees.

Table 2. Mean and standard deviation of the tree-asymmetry index of dendritic trees from different cell types.

Cell type	**Tree-asymmetry index $\overline{A_t}$ - Mean (SD)**	**Reference**
Rat cortical pyramidal basal	0.38 (0.22)	Van Pelt et al., 1992
Rat multipolar nonpyramidal	0.43 (0.26)	Van Pelt et al., 1992
Rat cerebellar Purkinje	0.492 (0.020)	Van Pelt et al., 1992
Spinal motoneurons (rat, cat, frog)	0.42 - 0.47	Dityatev et al., 1995
Cat superior colliculus (deep layer)	0.41 (0.15)	Van Pelt et al., 2001a
S1-rat cortical Layer 2/3 pyramidal	0.41 (0.24)	Van Pelt et al., 2001b
Guinea pig cerebellar Purkinje	0.50 (0.01)	Van Pelt et al., 2001b

3.2 Variation in the number of dendritic segments

The number of segments in dendritic trees shows large variations. In a study on terminal segment number distributions (Van Pelt et al., 1997) it was shown that the number of terminal segments per dendrite ranges from 1 up to about 50 in motoneurons in cat, rat or frog and from 1 up to about 15 in both rat pyramidal, multipolar nonpyramidal and in human dentate granule cells. The shape of the terminal segment number distributions turned out to be highly characteristic for the different cell types (see the figures in Van Pelt et al., 1997). Examples of such distributions for dendrites of 150 days old rat pyramidal and multipolar nonpyramidal cells, and of aged human fascia dantata granule cells are given in Figure 6.

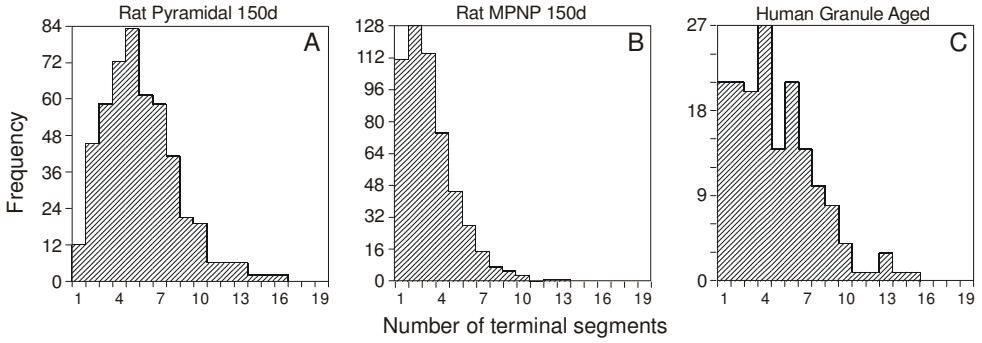

Figure 6. Frequency distributions of the number of terminal segments per dendritic tree for 150 days old rat cortical pyramidal (panel A) and multipolar nonpyramidal (MPNP) (panel B) cells (see Uylings et al., 1990) and for human fascia dentata granule cells (panel C) (De Ruiter and Uylings, 1987).

3.3 Variation in segment length

A large variation has been observed in the length of dendritic segments. A general observation is that terminal segments can be substantially longer than intermediate ones as for instance is shown in pyramidal cell basal dendrites of layer V with $\bar{l}_t$ = 117 (SD = 33) μm for terminal segments and $\bar{l}_i(median) = 11$ μm for intermediate segments (Larkman, 1991), in S1-rat cortical layer 2/3 pyramidal cell basal dendrites with $\bar{l}_t = 110.7$ (SD = 45.2) μm for terminal segments and $\bar{l}_i = 22.0$ (SD = 17.9) μm for intermediate segments (Van Pelt et al., 2001b) (see also Figure 7), in superior colliculus neurons with $\bar{l}_t = 115$ (SD = 83.3) μm and $\bar{l}_i = 80.3$ (SD = 75.5) μm (Schierwagen and Grantyn, 1986) and in rat Purkinje neurons with terminal segments having a length of about 13 μm

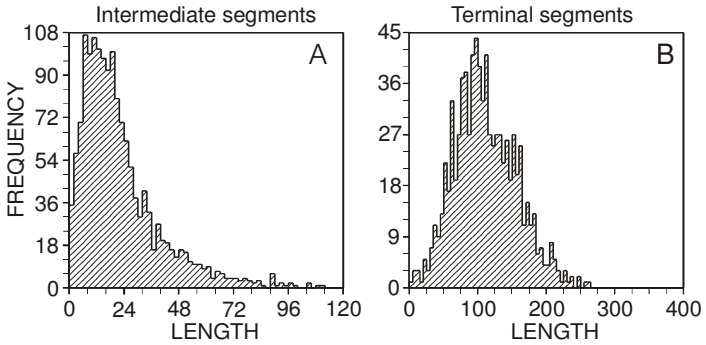

Figure 7. Frequency distributions of the length of (A) intermediate and (B) terminal segments of S1-rat cortical layer 2/3 pyramidal cell basal dendrites (Van Pelt et al., 2001b).

or 8 μm and intermediate segments having a length of about 5 μm (Woldenberg et al., 1993). An extensive review of intermediate and terminal segment lengths in dendrites of different cell types and species is given by Uylings et al. (1986, Table II). Additionally, terminal segment length may decrease strongly with increasing centrifugal order as is shown for instance by Uylings et al. (1978b). Van Veen and Van Pelt (1993) showed that such decrease in length as well as differences between intermediate and terminal segment lengths arise when the number and the positions of the branchpoints along the path from the soma to a terminal tip are determined by a Poisson process.

3.4 Variation in dendritic diameter

Dendritic segments have small diameters, down to the resolution of optical microscopes. The observed variation in segment diameters may therefore partly be attributed to measurement uncertainties. Nevertheless, a substantial part of the variation is induced by the different positions of the segments in the tree, caused by the correlation that is found between the diameter of a segment and its *degree* (Hillmann, 1988). The neuritic cytoskeleton is believed to be a major factor determining the diameter of dendritic segments. Hillman (1979, 1988) assumed a positive correlation between segment diameter and the number of microtubules. This correlation also results in a relation found between the diameters of a parent (d_p) and its daughter segments (d_1 and d_2) at a bifurcation, formulated by Rall (1959) as a power law relation

$$d_p^e = d_1^e + d_2^e \tag{6}$$

with e being the branch power parameter. Segment diameters thus decrease across bifurcation points with terminal segments having the smallest diameters. Terminal segments were found to have mean diameters of 1.1 μm for Purkinje cells (Hillman, 1979), 0.7 μm for pyramidal neurons (Hillman, 1979; Larkman, 1991), 0.7 (SD = 0.3) μm in cat phrenic motoneurons (Cameron et al., 1985) and about 1 μm for cat superior colliculus neurons (Schierwagen and Grantyn, 1986). Values for the branch power were reported of e = 2 for rat Purkinje and neocortical pyramidal neurons (Hillman, 1979), of $e = 1.47$ (SD = 0.3) (Schierwagen and Grantyn, 1986) for dendrites of cat superior colliculus neurons, of $1.5 < e < 2$ for rat visual cortex pyramidal neurons (Larkman et al., 1992), and of 3/2 for the distal parts of rat dentate granule cells (Desmond and Levy, 1984). Cullheim et al. (1987) found a value of 1.13 (SD = 0.34) for the mean ratio of $d_p^{1.5}/(d_1^{1.5} + d_2^{1.5})$ in cat α motoneurons.

4. MODELING DENDRITIC BRANCHING PATTERNS

In the *growth model approach* it is assumed that dendritic growth proceeds by branching and elongation of terminal segments. At a branching event a terminal segment is replaced by an intermediate one ending in a bifurcation point from which two new daughter segments emerge. Randomness is implemented by assigning branching probabilities and elongation rates to each terminal segment. The major challenge in this approach is to find (minimal) schemes for branching and elongation that result in model trees with similar geometrical properties as their observed counterparts. The model has been constructed step by step in the course of time, first concentrating on the topological variation between dendritic trees with equal number of terminal segments, secondly on the variation in the number of terminal segments per dendritic tree, and finally on the variation in segment length. Each step was accompanied by a thorough validation of the model outcomes with experimental data. The final model thus has a modular structure in which the

different parameters can be optimized for their corresponding shape properties in dendritic trees. The first step concerned the branching process only aiming at describing the observed frequency distribution of tree types with a given number of terminal segments (topological variation), as for instance shown in Figure 5. The second step aimed at describing the observed distribution of the number of terminal segments, as for instance shown in Figure 6. The third step concerned the joint branching and elongation process, aiming at describing segment length distributions, as for instance shown in Figure 7. These successive steps will be described in detail in the next sections.

4.1 Modeling topological variation (QS model)

Topological variation arises when branching events variably occur at different segments in the growing tree, such that each growth sequence, after a given number of branching events, may end in a different tree type. In the socalled QS-model, branching events were initially assumed to occur at both intermediate and terminal segments, with the selection probability of a segment for branching taken to depend on the type of the segment and on its centrifugal order. The selection probability p_{term} for branching of a terminal segment at centrifugal order γ is defined by $p_{term} = C_1 2^{-S\gamma}$, with parameter S modulating the dependence on centrifugal order, and C_1 being a normalization constant to make the sum of the branching probabilities of all the segments in the tree equal to one. For S = 0, all terminal segments have the same probability for being selected for branching. For S = 1, the branching probability of a terminal segment will decrease by a factor of two for each next centrifugal order. The selection probability of an intermediate segment p_{int} for branching relates to that of a terminal segment of the same order via $p_{\text{int}} = (Q/(1-Q))p_{term}$, with Q a parameter having values between 0 and 1. The parameter Q roughly indicates the total branching probability for all intermediate segments in a tree, with for Q = 0 branching of terminal segments only, and for Q = 1 branching of intermediate segments only. With the two parameters Q and S, a range of growth modes can be described, including the well-known random terminal mode of growth (*rtg*) with (Q,S) = (0,0) and the random segmental mode of growth (*rsg*) with (Q,S) = (0.5,0). An accurate description of the topological variability in dendrites from several neuron types and species could be obtained by assuming branching to occur at terminal segments only (i.e., Q=0), with possibly a slight dependence of the selection probability on the centrifugal order (small or zero value for S) (Van Pelt and Verwer, 1986; Van Pelt et al., 1992; Dityatev et al., 1995). The QS-model reduces to the S-model for Q = 0 and to the Q-model for S = 0. The probabilities of occurrence of tree types appear to depend strongly on the mode of growth. This is clearly shown in Figure 8, displaying the probabilities of trees of *degree* 8 for four different modes of growth, including *rtg* and *rsg*. Analytical expressions for the probabilities and expected values of some shape parameters could be obtained for the Q-model only. Dendritic growth according to the Q-model results in partition probabilities $p(r, n-r \mid Q)$ (i.e., probabilities for a tree of *degree n* to have first-order subtrees of *degrees r* and *n-r* given by

$$p(r,n-r \mid Q) = 2^{1-\delta(r,n-r)} \left\{ 1 + Q\left(\frac{n(n-1)}{2r(n-r)} - 2 \right) \right\} \frac{1}{n-1-Q} \prod_{i=1}^{r-1} \frac{1-Q/i}{1-Q/(i+n-r-1)} , \qquad (7)$$

$$p(1,n-1 \mid Q) = \frac{2+Q(n-4)}{n-1-Q} , \qquad (8)$$

$$\lim_{n\to\infty} p(1,n-1 \mid Q) = Q , \qquad (9)$$

$$p(r,n-r \mid rtg) = \frac{2^{1-\delta(r,n-r)}}{n-1} \ , \tag{10}$$

$$p(r,n-r \mid rsg) = \frac{N_\tau^r N_\tau^{n-r}}{N_\tau^n} 2^{1-\delta(r,n-r)} \tag{11}$$

(Van Pelt and Verwer, 1985) with δ denoting the Kronecker δ.

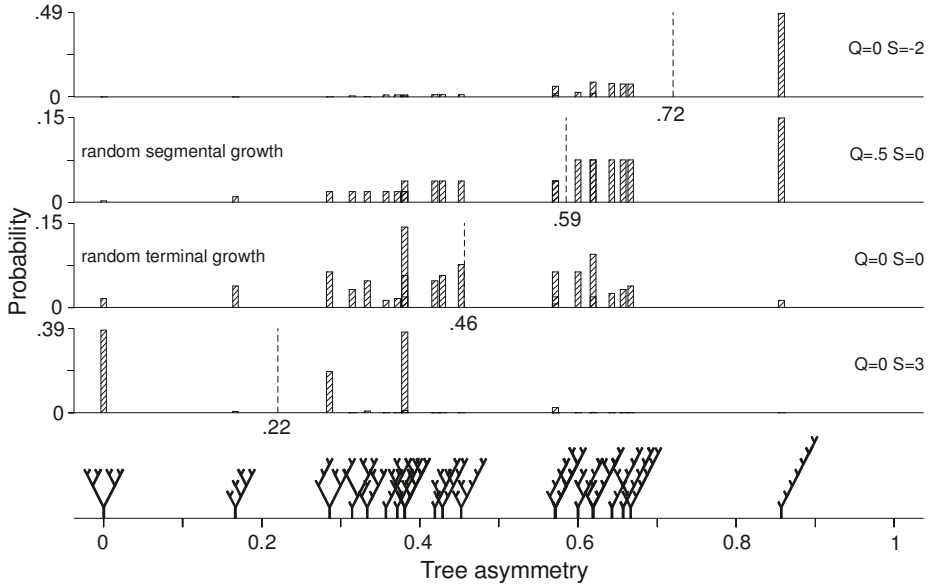

Figure 8. Plot of probabilities of occurrence of tree types of degree 8. The trees are plotted versus the tree-asymmetry values in the bottom row. The probabilities have been calculated for four different modes of dendritic growth, i.e., for (Q,S) = (0,-2) in the top row, the random segmental mode of growth (Q,S) = (0,0.5) in the second row, the random terminal mode of growth (Q,S) = (0,0) in the third row, and for (Q,S) = (0,3) in the fourth row. The mean value of the tree-asymmetry index for a given mode of growth is indicated by a dotted line. The figures demonstrate that the tree-type probabilities and the tree-asymmetry expectations depend strongly on the mode of growth. Note, that probability bars of trees with equal asymmetry index do overlap.

The tree-asymmetry expectation for the random terminal growth mode (*rtg*) is given by

$$E\{A_t^n \mid rtg\} = \frac{2n}{3(n-1)} \left\{ \frac{2-3n_e/n}{4(n_e-1)} - \frac{2}{n_e} + \sum_{k=n_e/2}^{n_e} \frac{1}{k} \right\} \tag{12}$$

with $n_e = n - \varepsilon(n)$ and $\varepsilon(n)$ defined in Equation (2).

$$\lim_{n\to\infty} E\{A_t^n \mid rtg\} = -\frac{1}{3} + \sum_{k=1}^{\infty} \frac{1}{(k+1)(2k-1)} = \frac{2}{3}\ln 2 = 0.4621 \tag{13}$$

(Van Pelt et al., 1992). For the random segmental growth mode (*rsg*) is the tree-asymmetry expectation given by

$$E\{A_t^n \mid rsg\} = \frac{2}{(n-1)N_\tau^n} \sum_{m=2}^{n} \frac{2(n-m)-1}{m-2} N_\tau^{n-m} \times \sum_{r=1}^{m/2} \{2-\delta(r,m-r)\}(m-2r) N_\tau^r N_\tau^{m-r} \qquad (14)$$

(Van Pelt et al., 1992). These expectations (mean values) are indicated in Figure 8 by the dotted lines for the displayed modes of growth.
The QS model has been used to analyse dendrites from a variety of neuronal cell types and species (Van Pelt et al., 1992; Dityatev et al., 1995). In all cases optimized parameter values could be found so as to accurately reproduce the observed topological variation. A given value for the mean asymmetry index, however, is not uniquely associated with a particular combination of QS values, but with a contour in QS-space. For values of the asymmetry index smaller than about 0.5, the contours remain close to the S-axis. All contours start at the S-axis, implying that the S-axis (Q = 0) is able to generate a full range of asymmetry expectations (Van Pelt et al., 1992). At present, all reported asymmetry values for neuronal dendrites are smaller than or equal to 0.5 (see also Table 2). Therefore, we assume in the following that Q = 0, i.e., that branching occurs at terminal segments only, while the probability for a terminal segment to be selected may depend slightly on its position in the tree (i.e., its centrifugal order).

4.2 Modeling the variation in the number of terminal segments per dendrite (BE-, BES- and BEST model)

Variation in the number of segments per dendritic tree emerges when trees experience a variable number of branching events during a particular period of outgrowth. In the socalled BE-growth model (Van Pelt et al., 1997) it is assumed that branching events occur at random points in time and at terminal segments only. To this end, the developmental time period is divided into a number of N time-bins with not necessarily equal durations. In each time-bin *i* a terminal segment in the tree may branch with a probability given by

$$p_i = B / N n_i^E \qquad (15)$$

with the parameter B denoting the expected number of branching events at an isolated segment in the full period, and the parameter E denoting the dependence of the branching probability of a terminal segment on the total number of terminal segments n_i in the growing tree. Equation 15 can also be written as $p_i = D n_i^{-E}$ with $D = B/N$ denoting the branching probability per time bin of an isolated terminal segment. The duration of the time-bins is taken sufficiently small (i.e., the number of time-bins sufficiently large) so as to make the branching probabilities p_i much smaller than one, and making the probability for more than one branching event per time bin in the tree negligibly small. For $E = 0$, the branching probability is constant, independent of the number of terminal segments in the tree.

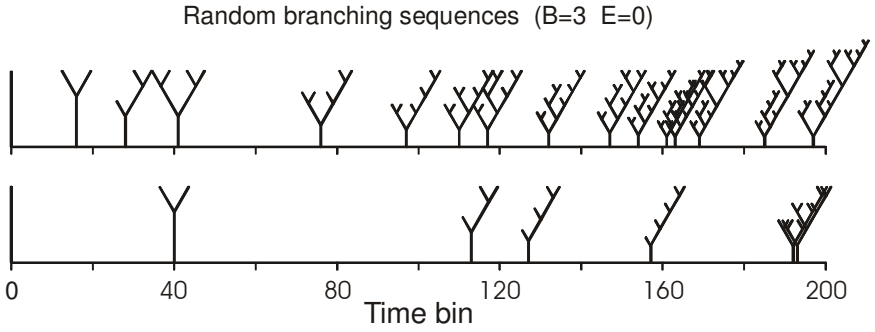

Figure 9. Two examples illustrating the growth of a branching pattern for the parameter values B = 3 and E = 0. The full time period is divided into N = 200 time bins. At each time bin, any of the terminal segments in the growing tree may branch with a constant probability. The trees are plotted at the time bin where a branching event has occurred.

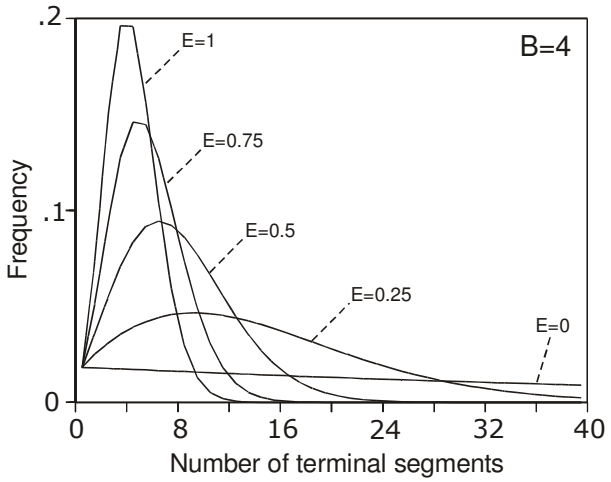

Figure 10. Degree distributions of trees obtained by growth modes with B = 4 and different values for the parameter E, i.e., with different dependencies of the branching probability of a terminal segment on the total number of terminal segments in the tree. For E = 0, the distribution is monotonically decreasing and has a long tail. For increasing values of E, the distributions get a modus and become increasingly narrower.

Examples of growth sequences are given in Figure 9 for parameter values B = 3 and E = 0. The two sequences show the random occurrences of branching events in time as well as the difference in the number of terminal segments in the final trees. Additionally, they show that the number of branching events in the full period can be (much) larger than the value of B = 3, because of the proliferation in the number of terminal segments during growth. The variation in terminal segment number is most clearly shown in Figure 10 in which the distribution functions are displayed of the number of terminal segments per dendritic tree in sets of trees obtained for B = 4 and for different values of the growth parameter E. For E = 0, the distribution is monotonously decreasing with increasing number of terminal segments and has a long tail. For $E > 0$, the distributions become unimodal, and increasingly narrower while long tails disappear for increasing values of E.

The distribution of the number of terminal segments in dendritic trees after a period of growth can be calculated by means of the recurrent expression

$$P(n,i) = \sum_{j=0}^{n/2} P(n-j, i-1) \binom{n-j}{j} [p(n-j)]^j [1-p(n-j)]^{n-2j} \qquad (16)$$

(Van Pelt et al., 1997) with $P(n,i)$ denoting the probability of a tree of *degree* n at time bin i with $P(1,1)=1$, and $p(n)$ denoting the branching probability per time-bin of a terminal segment in a tree of *degree* n, with $p(n) = Bn^{-E} / N$. A tree of *degree n* at time-bin *i* emerges when *j* branching events occur at time-bin *i-1* in a tree of degree *n-j*. The recurrent equation expresses the probabilities of all these possible contributions from j = 0, ..., n/2. The last two terms express the probability that, in a tree of *degree n-j*, *j* terminal segments will branch while the remaining *n-2j*

terminal segments will not do so. The combinatorial coefficient $\binom{n-j}{j}$ expresses the number of possible ways of selecting *j* terminal segments from the existing *n-j* ones. A continuous time implementation of this recurrent equation has recently been described by Van Pelt and Uylings (2002). The BE model has shown to be able to reproduce accurately the shape of terminal segment number distributions from dendrites of different cell types and species (Van Pelt et al., 1997). Optimal parameter values were found of $(\overline{B}(sem), \overline{E}(sem))$ = (3.55 (0.17), 0.68 (0.02) or rat pyramidal cell basal dendrites, of (3.92 (0.4), 0.29 (0.04)) for the combined group of motoneurons from cat, rat and frog, of $(\overline{B}, \overline{E})$ = (2.36, 0.38) for human dentate granule cells, of $(\overline{B}, \overline{E})$ = (21.49, 0.42) for rat multipolar nonpyramidal cells, and of (50, 0.54) for 1 month rat cerebellar Purkinje cells.

Including topological variation into the BE-model (BES-model)}

In the BE-model all terminal segments have equal probability for branching and the topological variation, produced by the BE-model is similar to that produced by the random terminal growth mode (Q=0, S=0). An account of the topological variability can now be given in a combined BES-model by taking the branching probability of a terminal segment per time-bin p_i also dependent on the centrifugal order of the segment, like in the S-model, such that

$$p_i = C2^{-S\gamma} B / Nn_i^E \qquad (17)$$

with γ denoting the centrifugal order of the terminal segment and $C = n / \sum_{j=1}^{n} 2^{-S\gamma_j}$ being a normalization constant, with a summation over all *n* terminal segments. The normalization ensures that the summed branching probability per time-bin of all the terminal segments in the tree is independent of the value of *S*.

Modeling branching process in real time (BEST model)

The time bins have been introduced without specifying their durations. To calculate the branching process in real time, the time-bin scale has to be mapped onto the real time scale. The branching probability per time bin $p_i = Dn_i^{-E}$ then transforms into a branching probability per unit of time $p(t) = Dn_i^{-E} / \Delta T_i$ with ΔT_i being the duration of time bin *i*. A linear mapping involves equal durations of the time bins. A typical example of a growth curve of the terminal segment number per dendrite is given in Figure 11. It shows how the mean and standard deviation increase in time. Also the growth rate increases with the highest value at the end of the period. The branching probability per unit of time, however, declines in time, because of the increasing number of terminal segments in the growing tree.

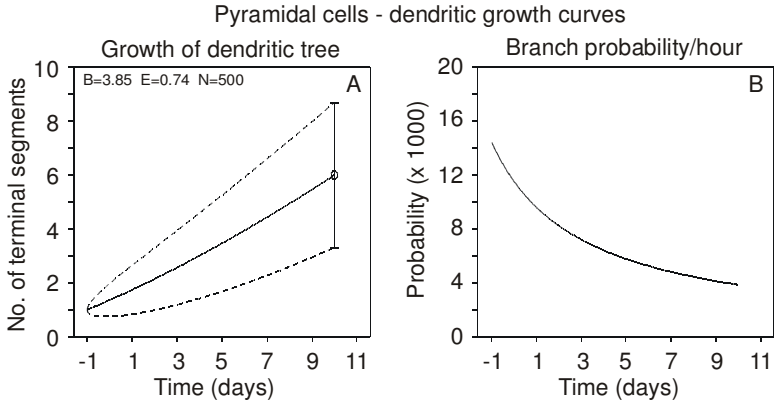

Figure 11. Growth curve of the mean terminal segment number in dendritic trees for the growth mode B = 3.85, E = 0.74. The dashed lines indicate the standard deviation intervals around the mean. The right panel indicates how the branching probability per hour declines with age because of the increasing number of terminal segments and the non-zero value of E.

A non-linear mapping of the time bins to real time modifies the shape of the growth curve, but, importantly, does not change the relation between mean and standard deviation. Therefore it offers the possibility to adapt the growth curve to a set of observed values at different points in time for the mean and standard deviation (see Van Pelt et al., 1997 for an example of Purkinje cell development). A non-linear mapping of the time bin scale has as consequence that the constant D transforms into a non-linear function of time $D(t)$, also called the baseline branching rate function. Recently, the dependence of the dendritic growth function on the baseline branching rate function $D(t)$ has been described in detail by Van Pelt and Uylings (2002). Using a developmental data set of Wistar rat layer IV multipolar nonpyramidal neurons, it was shown that an exponential decreasing baseline branching rate function with a decay time constant of τ =3.7 days resulted in a terminal segment number growth function that matched the observed data very well.

Table 3. Developmental and shape characteristics of basal dendrites of large layer V rat cortical pyramidal neurons.

Onset of branching/elongation	≈ day 1 (24 h) an	Uylings (unpub. observations)
Stop of branching	day 10 (240 h) pn	Uylings et al., 1994
Stop of elongation	day 18 (432 h) pn	Uylings et al., 1994
# terminal segments per dendrite	6.0 (SD = 2.7)	Larkman, 1991
Intermediate segment length	11 (median) µm	Larkman, 1991
Terminal segment length	117 (SD = 33) µm	Larkman, 1991
Pathlength to tips	156 (SD = 29) µm	Larkman, 1991
Total dendritic length	777,6 µm	*
Terminal segment diameter	0.8 (SD = 0.2) µm	Larkman, 1991
Branch power	1.5 < e < 2	Larkman et al., 1992
Tree asymmetry	0.38 (SD = 0.22)	Van Pelt et al., 1992

Abbreviations: *an* before birth, *pn* after birth.

* The mean total length per dendritic tree of 777.6 µm is estimated from the total basal dendritic length per pyramidal neuron of 4.510 mm (Larkman and Mason, 1990), and the mean number of basal dendrites per pyramidal neuron of 5.8 (SD = 1.8) (Larkman, 1991).

4.3 Modeling the variation in the length of dendritic segments (BESTL model & Simulation procedure)

4.3.1 *BESTL model*

Segment lengths are determined by both the rate of elongation and branching of terminal segments. In the previous section it was shown that the parameters of the branching process can be estimated from the dendritic segment number distribution. Segment elongation thus needs to be included in the branching process for studying segment lengths, as will be illustrated for the growth of dendrites of large layer V rat cortical pyramidal neurons. The relevant empirical findings for these neurons are summarized in Table 3. Note, that growth starts one day before birth, and continues with branching up to day 10, while the elongation of segments continues up to day 18 (Uylings et al., 1994).
The topological variation was well described for the model parameters Q = 0, S = 0.87 (Van Pelt et al., 1992). The terminal segment number distribution was well reproduced by the branching process parameters B = 3.85 and E = 0.74 (Van Pelt et al., 1997) (see also Table 4). Equal time-bins or, similarly, a constant function *D*, will be assumed. For the elongation rate of terminal segments we initially assume a fixed value of 0.34 μm/h, estimated from the mean pathlength of 156 μm traversed in the total period of growth of 456 h. With these model parameters and including different stop times for the branching and elongation process, dendrites were produced with mean values for their intermediate and terminal segment lengths of 23.6 (SD = 18.9) (median = 18.8) and 96.0 (SD = 22.1) μm, respectively. These values are longer, respectively, shorter than the observed values of 11 (median) and 117 (SD = 33) μm, indicating that the assumption of constant segment elongation gives incorrect results. Branching terminates at 240 hours postnatal. Terminal segments become longer when the growth cones propagate faster during the elongation phase.

Table 4. Parameter values used for modeling the growth of basal dendrites of large layer V rat cortical pyramidal neurons. The second column indicates which parameters were used for optimizing the shape parameters in the third column to the observed values (indicated as free parameters), and which ones were directly derived from observed data.

Parameter	**use**	**Optimization on**
B = 3.85	free	*degree* mn,sd
E = 0.74	free	*degree* mn,sd
V_{el} = 0.51 μm/h	free	mean terminal segment length
cv in prop. rate = 0.28	free	sd in pathlength
V_{br} = 0.22 μm/h	calculated	*
T_{onset} = -24 h	observed	
T_{bstop} = 240 h	observed	
T_{lstop} = 432 h	observed	

T_{onset}, T_{bstop} and T_{lstop} denote the time of onset of branching and elongation, the stop time of branching, and the stop time of elongation, respectively.
* The mean elongation rate during the branching phase V_{br} is calculated from the optimized value for the elongation rate during the elongation phase V_{el}, the durations of the branching phase $T_{br} = T_{bstop} - T_{onset}$ = 264 h and elongation phase $T_{el} = T_{bstop} - T_{bstop}$ = 192 h and the mean pathlength L_p = 156 μm by means of $V_{br} = (L_p - V_{el} \times T_{el}) / T_{br}$.

To maintain the same mean elongation rate during the total developmental period this implies a slower rate during the branching phase. Next, elongation rates of 0.22 μm/h during the branching

phase and of 0.51 μm/h during the elongation phase were taken, still without variation in these rates. These runs resulted in dendrites with mean (SD) values for the intermediate and terminal segment lengths of 15.2 (SD = 12.2) μm, (with median = 12.1) and 117.4 (SD = 14.2) μm, respectively, and pathlengths of 156 μm without variation. The mean values are now in good agreement with the observed values. Note, that the standard deviations in the segment lengths are solely due to randomness in the branching process, and are smaller than the observed values. In the final simulation run randomness was incorporated in the elongation rate by assigning, at the time of birth of a growth cone after a branching event, a random value from a normal distribution with mean 0.22 μm/h during the branching phase and 0.51 μm/h during the elongation phase, and with a coefficient of variation (cv) of 0.28. With this cv value it was found that the model-predicted standard deviation in the pathlength distribution optimally matches the observed value of 29 μm. A summary of the parameter values is given in Table 4.

An example of a growing dendrite is given in Figure 12. The dendrite is displayed at successive days of its development. Note, that branching terminates 11 days after onset and is followed by a period of elongation only.

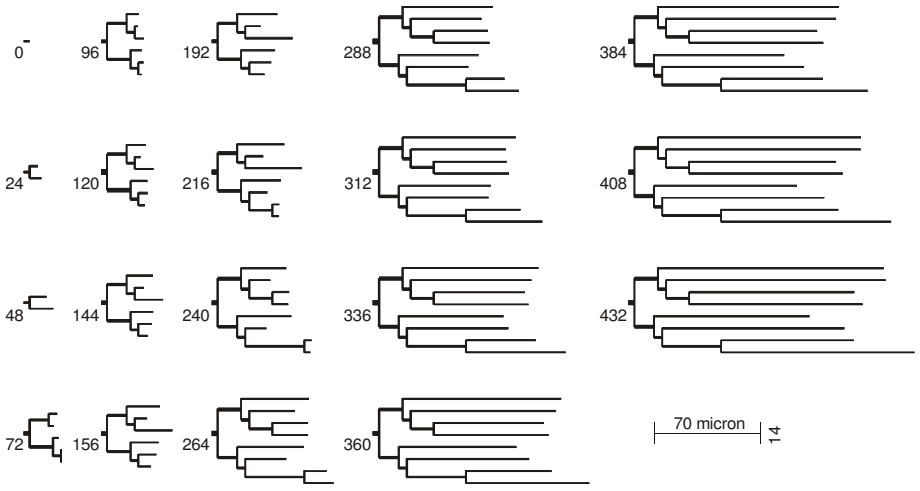

Figure 12. Plot of a model dendritic tree at successive days of its development (the numbers at the root denote the postnatal time in hours). The growth parameters used were optimized for basal dendrites of large layer V rat cortical pyramidal neurons and given in Table 4. A period of branching and elongation from one day before birth up to 10 days after birth (denoted as branching phase) is followed by a period of elongation only up to day 18 (denoted as elongation phase). Different elongation rates are assumed of 0.22 μm/hour in the branching phase and 0.51 μm/hour in the elongation phase.

Typical examples of random full grown dendritic trees, at the end of their developmental period, are shown in Figure 13. The statistical shape properties of the model dendrites are summarized in Table 5 and are in good agreement with the observed data both in the mean and in the standard deviation. In the last column it is indicated whether the agreement is the result of the optimization of the model parameters or an emergent outcome of the model ("prediction"). The agreement between the predicted and observed values underscores the validness of the model and its underlying assumptions.

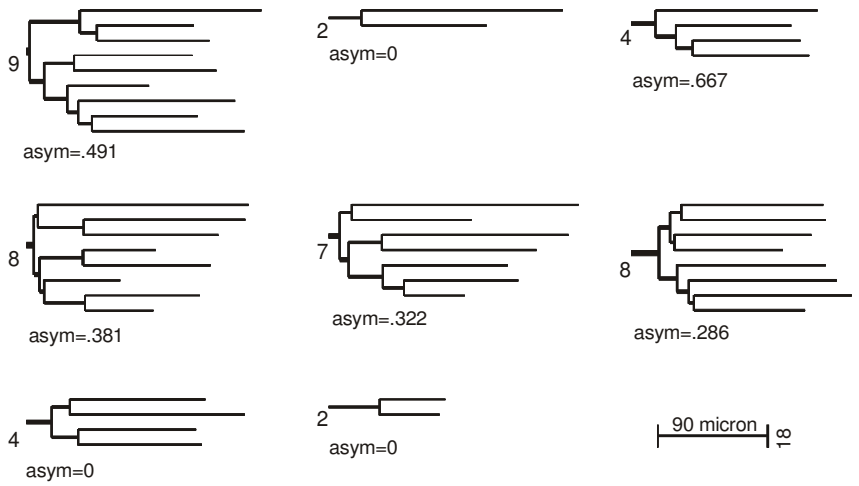

Figure 13. Examples of full grown model dendrites obtained for model parameters given in Table 4, which were optimized for basal dendrites of large layer V rat cortical pyramidal neurons. For each tree, the number of terminal segments is given as well as the tree asymmetry index (asym).

Table 5. Shape properties of model dendrites grown by means of the growth model for the parameter values given in Table 4. See the text for description of the model. In the last column is indicated which shape variables were matched to the observed values by optimizing the model parameters (see Table 4) and which shape variables are just outcomes of the growth model and can be considered as predictions for further empirical verification.

Shape variables		**Obs.**	**Model outcomes**	
Degree	mn	6.0	6.0	optimized
	Sd	2.7	2.7	optimized
Asymmetry	mn	0.38	0.36	optimized
	Sd	0.22	0.20	*prediction*
Centrifugal order	mn		2.26	*prediction*
	Sd		1.24	*prediction*
Total length	mn	777.6	774.6	*prediction*
	Sd		342.9	*prediction*
Terminal length	mn	117	117.1	optimized
	Sd	33	31.4	*prediction*
Intermediate length	mn		15.4	*prediction*
	Sd		13.4	*prediction*
	Median	11	11.6	*prediction*
Pathlength	mn	156	156.2	estimated
	Sd	29	29.2	optimized

The obtained distributions for several shape parameters are shown in Figure 14. The terminal segment number distribution closely corresponds to the observed one, as is shown in Van Pelt et al., (1997). Unfortunately, experimental distributions for the other parameters were not available. The distribution of the tree-asymmetry values shows the irregular pattern, characteristic for the discrete tree types and a mean value of 0.36 that is typical for the S = 0.87 mode of growth (i.e., random branching of terminal segments with a slight preference for the proximal ones). The

simulations without and with variation in elongation rates make clear which part of the variation in segment lengths and total dendritic lengths is due to randomness in branching and which part is due to randomness in elongation. Note, that the optimized value of 0.28 for the coefficient of variation in the elongation rate is larger than the value of 0.186 (= 29/156) for the observed pathlength distribution. The reason is that pathlengths in a dendritic tree are not independent from each other because paths to terminal tips share common intermediate segments (for instance, all paths have the root segment in common).

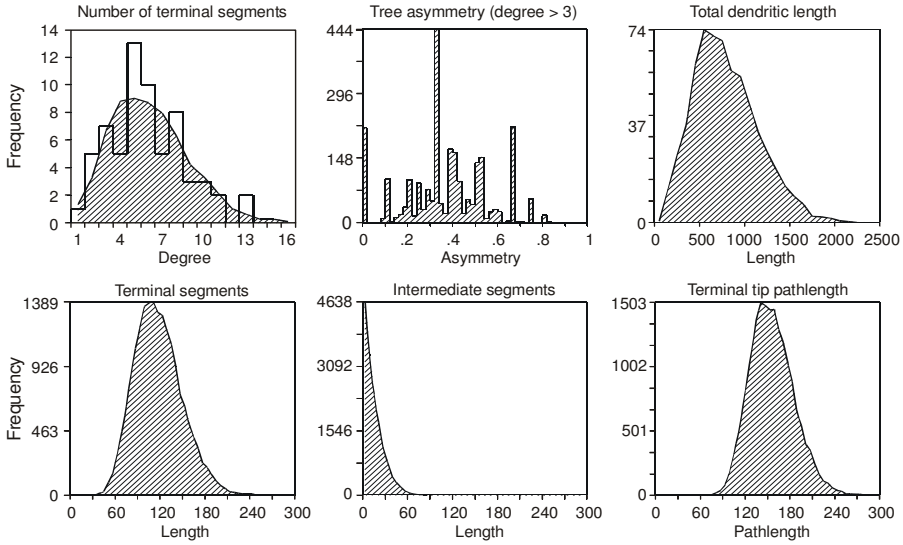

Figure 14. Model distributions (shaded) of the shape parameters *degree*, *tree asymmetry*, *total dendritic length*, *terminal segment length, intermediate segment length* and *terminal tip pathlength* of model dendrites generated with parameter values given in Table 4. The values of the mean *mn* and standard deviation *sd* are given in Table 5. The first panel also includes the observed distribution of the number of terminal segments.

The intermediate segment length distribution of the model trees has an exponential shape (Figure 14). Experimental distributions of other cell types with higher resolution, however, show clear cut modal shapes (e.g., Nowakowski et al., 1992; Uylings et al., 1978a, 1994), and also shown in Figure 7. Apparently, short intermediate segments in dendritic reconstructions do occur less frequently than expected. Nowakowski (1992), who first noticed this finding, assumed a transient suppression of branching immediately after a branching event. To account for this observation without interfering with the branching scheme, we have alternatively assumed that newly formed segments after a branching event have an initial length when stabilized and able to form subsequent branches. This additional assumption resulted in accurate reproductions of the observed intermediate segment length distributions (Van Pelt et al., 2001a; 2001b; 2003). Additionally, the baseline branching rate function *D(t)* may not be constant but a decreasing function of time, as was recently shown for rat cortical multipolar non-pyramidal dendrites (Van Pelt and Uylings, 2002). Such a function will also have implications for the segment length distributions. Unfortunately, neither the initial length nor the nonlinear function *D(t)* could be incorporated in this analysis of the large layer V cortical pyramidal neurons because the experimental data set of this cell group (Larkman, 1991) did not included experimental segment length distributions.

The implication of a nonlinear baseline branching rate function for the metrical development of dendritic trees has recently been studied by Van Pelt and Uylings (2003). Using a developmental data set of Wistar rat layer IV multipolar nonpyramidal neurons, it was shown that an exponential decreasing baseline branching rate function with a decay time constant of τ =3.7 days resulted in a total tree length growth function that matched the observed data very well.

Agreement between experimental and modeled distributions of dendritic shape parameters has now been obtained for a variety of cells types and species, viz., rat cortical layer 5 pyramidal neuron basal dendrites (Van Pelt and Uylings, 1999), S1 rat cortical layer 2/3 pyramidal neurons (Van Pelt et al., 2001b), guinea pig cerebellar Purkinje cell dendritic trees (Van Pelt et al., 2001b), cat superior colliculus neurons (Van Pelt et al., 2001a), Wistar rat visual cortex layer IV multipolar nonpyramidal neurons (Van Pelt et al., 2003), Wistar rat layer 2/3 associative pyramidal neurons (Granato and Van Pelt, 2003), and for terminal segment number distributions only in Van Pelt et al. (1997). Optimized model parameter values are summarized in Van Pelt et al. (2001c).

4.3.2 *Simulation procedure*

The simulation of the growth process for the BESTL-growth model includes the following steps:

1. Parameter S is estimated from the topological variation in the observed trees (see Van Pelt et al., 1992).

2. Parameters B and E are estimated from the observed *degree* distribution (see Van Pelt et al., 1997).

3. The baseline branching rate function *D(t)* has to be estimated. When experimental data is available for the number of terminal segments at several developmental time points one may follow two approaches. The first one is to find a (non)linear mapping of the time bins onto real time (see Van Pelt et al., 1997; and Van Pelt and Uylings (2002)), such that the model growth curve predicted for constant D transforms into a curve that matches the observed data. Then, using the bin-to-time mapping, each time bin corresponds to a time period for which the function $D(t) = B / \Delta T(i) N$ can be calculated. In the second approach an analytical baseline branching rate function is assumed (e.g. an exponential one) and its parameters are subsequently optimized by fitting the predicted terminal segment number growth function to the observed one (detailed examples of these different approaches are given in Van Pelt and Uylings, 2002). When the observed dendrites originate from only one point in time, the shape of the baseline branching rate function has to chosen (e.g. a linear or exponential one).

4. Trees are now generated according to the following iterative algorithm: For a given tree at a given point in time t, the branching probabilities are calculated for all of the *n(t)* terminal segments with, for $S \neq 0$, the centrifugal order γ being taken into account of each of them, using $p(t) = C(t) 2^{-S\gamma} D(t) n(t)^{-E}$. The normalization constant $C(t)$ is obtained via $C(t) = n(t) / \sum_{j=1}^{n(t)} 2^{-S\gamma_j}$. Then, using a uniform random number between 0 and 1, it is decided for each terminal segment whether a branching event actually occurs in the present time step (i.e., a branching event occurs when the random number is smaller than or equal to the branching probability for that segment). A branching event implies that the terminal segment becomes an intermediate segment ending in a bifurcation with two daughter terminal segments, which are given an initial length and an elongation rate. These values are obtained by random sampling gamma distributions with means and standard deviations as given for the initial length and for the elongation rate for that point in time, respectively. All terminal segments (including the new ones) are subsequently elongated according to their individual rates. The process starts at the time of onset with a single (root) segment and stops at the last point in time (see also Van Pelt et al., 2001b).

4.4 Modeling the variation in segment diameter

No developmental rules have so far been used to generate the diameters of segments. The segment diameters in the displayed dendrograms have therefore been estimated by assuming a power law relation. By the power law relation, the diameter of an intermediate segment (d_s) is determined by the number of terminal segments n_s in its subtree according to $d_s^e = n_s d_t^e$ or $d_s = d_t n_s^{1/e}$. Accordingly, the diameter of a segment in a growing tree is expected to increase with the increasing number of terminal segments. The segment diameters in a tree have been estimated by means of the following procedure. First, terminal segment diameters are estimated by random sampling the observed terminal segment diameter distribution (or a normal distribution based on the observed mean-sd values). At each bifurcation the diameter of the parent segment is estimated by using a branch power value obtained by random sampling the observed branch power distribution. For the dendrograms in Figures 12 and 13 the terminal segment diameters were randomly sampled from a normal distribution with mean 0.8 μm and standard deviation 0.2 μm (Larkman, 1991). The branch power distribution was assumed to be a normal one with mean 1.6 and standard deviation 0.2 (values estimated from Larkman et al., 1992).

5. DISCUSSION

The growth model for dendritic trees, discussed here, is based on a stochastic description of branching and elongation of terminal segments. The model is able to reproduce dendritic complexity with respect to number, connectivity and length of dendritic segments. It should be noted that both branching and elongation determine the length of segments, such that their distributions can only be studied by taking both processes into account. The agreement between model outcomes and empirical data was obtained for a larger number of shape parameters than the number of optimized model parameters, giving further support to the assumptions made in the model. Five aspects have been distinguished in dendritic growth, viz., (i) the baseline branching rate function *D(t)* of individual growth cones; (ii) the 'proliferation' of the number of growth cones in the growing tree *n(t)*; (iii) the 'modulation' of the branching probability by the increasing number of growth cones (determined by the parameter *E*) and the position of the segment in the tree (via parameter S); (iv) the elongation of segments by the migration of growth cones, and (v) the assignment of initial lengths to newly formed segments after branching.

Because of the structure of the model, both its parameters (i.e., the rates of branching and migration of growth cones) and its outcomes (i.e., the generated dendrites and the distributions of their shape parameters) can directly be associated with the biological processes and structures. This enables the empirical validation of its assumptions and outcomes. The model has shown to be able to accurately reproduce dendritic geometrical properties of a variety of neuronal cell types. Dendritic growth is a complex process, mediated by the dynamic behavior of growth cones showing periods of forward migration but also of retraction. On a short time scale these actions are implicitly accounted for by the stochasticity of the model. On a longer time scale, changes in growth cone behavior can be described by specifying the time profile of the baseline branching rate function, and of the migration rates. Such specification, however, requires the availability of experimental data of dendritic shapes at more than one point in time. For instance, in the present example different segment elongation rates were assumed during the two phases of development. Dendrites may also experience phases of remodeling, when the number of segments substantially reduces. Dendritic regression is not included in the present model, but may be incorporated with an unavoidable increase in complexity of the model. In a study on the impact of pruning on the topological variation of dendritic trees, Van Pelt (1997) showed that under uniform random pruning

schemes the topological variance of the pruned trees remained consistent with the mode of initial outgrowth.

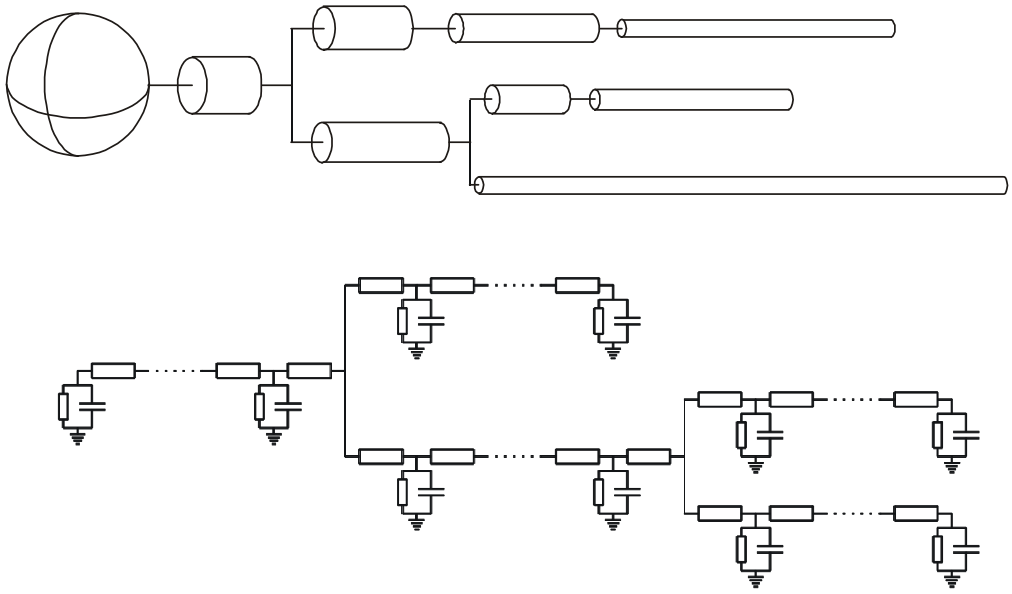

Figure 15. (top) Example of a branching cable model in which each segment is modeled as one or more cylindrical membranes and (bottom) a compartmental model in which each segment is modeled as a series of isopotential R-C compartments. (Figure drawn after Figure 3.3 in Koch and Segev (1989)).

The progress in modeling dendritic structure makes it also possible to study systematically the functional implications of realistic morphological variations. Since the pioneering work on cable theory of Rall (see e.g. Rall et al., 1992; Rall, 1995) many methods have been developed for studying the processing of electrical signals in passive and active dendritic trees. Both the branching cable and the compartmental models (e.g., Koch and Segev, 1989; see also Figure 15) have made it clear how signal processing depends on dendritic structure and membrane properties. The impact of topology on input conductance and signal attenuations in passive dendritic trees has first been studied systematically by Van Pelt and Schierwagen (1994; 1995). The use of one single vector equation for the whole dendritic tree, including the Laplace-transformed cable equations of all the individual segments, greatly simplified and accelerated the electrotonic calculations (Van Pelt, 1992). These studies demonstrated how dendrites with realistic topological structures differ in their passive electrotonic properties from symmetrical trees, and how the natural topological variation in dendritic morphologies contributes to the variation in functional properties. Regarding the influence of morphology on dendrites with active membrane, it was shown by Duijnhouwer et al. (2001) that dendritic shape and size differentiates the firing patterns from regular firing to bursting, when the dendrite is synaptically stimulated randomly in space and time. Similar effects of dendritic shape under conditions of somatic stimulation with fixed current injections were earlier reported by Mainen and Sejnowski (1996). Systematic studies of the effect of dendritic topology on neuronal firing have shown that firing frequency correlates with the mean dendritic pathlength (Van Ooyen et al., 2002) when the neuron is stimulated at the soma, while the type of firing (bursting or regular) is strongly influenced by dendritic topology when neurons are activated by synaptic stimulation of the dendritic tree (Van Elburg et al, personal communication). In these topological studies all the dendrites were given the same metrical and membrane properties. Schaefer et al. (2003) found that the detailed geometry of proximal and distal oblique dendrites

originating from the main apical dendrite in thick tufted neocortical layer 5 pyramidal neurons determines the degree of coupling between proximal and distal action potential initiation zones. Coupling is important for coincidence detection as it regulates the integration of synaptic inputs from different cortical layers when coincident within a certain time window. They conclude that dendritic variation may even have a stronger effect on coupling than variations in active membrane properties.
All these studies indicate that morphological variability of neurons may be an important contributor to their functional differentiation, keeping in mind that such approaches reflect a caricature of the natural branching structure (see Fig. 15). Further insight in the subtleties of active neuronal processing of electrical signals and information is needed to fully clarify the functional implications of morphological details and variations. However, it is clear that integration in the brain is one such subtlety or "bug" that arises from intricate biological variability, irrespective of the computational capabilities a neuron is thought to possess (cf. Vetter et al., 2001; Schaefer, 2003).

Dendritic shapes have been studied in this chapter by focusing on the metrics and connectivity of the individual segments (see Section 2). Clearly, dendrites are 3D structures with a particular embedding in 3D space, and further shape descriptors are needed for their full 3D characterization, such as the angles between segments at bifurcation points, the curvature of the segments, and multiscale fractal measures (e.g., Costa et al., 2002). Recent developments in modeling 3D dendritic geometry now also concern dendritic orientation in 3D and environmental influences (Ascoli et al., 2001; Ascoli, 2002a). The 3D dendritic geometry gets functional implications when the extracellular space participates in the electrical circuitry in an inhomogeneous manner and/or when dendrites are connected to each other via electrical contacts (for instance via gap junctions) (e.g. Poznanski et al., 1995). It is expected that the proximity of dendritic branches becomes an important aspect in dendritic 3D geometry, for which the topological structure and the angles between branches at bifurcation points are crucial parameters. The present equivalent cylinder -, branching cable - and compartmental models, however, do not incorporate these 3D aspects.

6. CONCLUSIONS AND FUTURE PERSPECTIVES

The mathematical modeling of dendritic growth using a stochastic description of growth cone behavior has brought many dendritic shape parameters and their variations into a coherent framework. It allows for analysis of dendritic shapes in terms of their developmental histories and for predictions of growth cone branching and elongation. Importantly, the model provides a useful tool for generating sets of randomly varying dendritic trees for use in studies of the functional implications of morphological variations. Both metrical and topological aspects of dendritic shapes have to be incorporated in assessing how the dendrite integrates in space and time the trains of incoming post synaptic potentials resulting in particular series of generated action potentials. Clearly, also membrane properties are subjected to variations as for instance caused by the types and the spatial distributions of the membrane channels, which contribute to the individual functional properties of the particular dendrite. Additionally, a neuron is a highly complex dynamic system and many structural aspects of the system have time dependent properties with large ranges of time constants, like for instance activity-dependent influence on membrane conductances (e.g., Abbott and LeMasson, 1993) and neurite outgrowth (e.g., Van Ooyen 1994). The integrative properties and firing characteristics are therefore expected to depend on the dynamic history of the neuron in a very complex manner.

It is expected that structural cable models become increasingly important in future studies of dendritic structure-function relationships. Structural cable models will also need to describe dendritic morphologies with increasing natural detail, in order to get better understanding of the

rich dynamic repertoire of dendritic operation. A typical example of greater realism is the 3D dendritic geometry and the embedding in the neuropil. For the modeling of 3D geometry also the angles between the segments at bifurcation points and the curvature of the segments should therefore be taken into account. For the growth model it would require the migration of growth cones to proceed in 3D as well as a qualification of the 3D environment of the outgrowing neurites. The presented growth model in this chapter for generating branching patterns with realistic topological and metrical variations contribute to this development and allows such future extensions quite naturally.

PROBLEMS

1. Real dendrites are structures embedded in 3D space having irregular branches and orientations. How can these morphological aspects best be built into the growth model? The growth process needs to be formulated in 3D space, with specific assumptions for the direction of outgrowth of growth cones. New possibilities are then offered for validating these assumptions using observed orientation and irregularity properties of dendritic branches.
2. The growth cone branching probability has been formulated as a function of the total number of growth cones, a position dependent term and a baseline branching rate representing all other factors determining the branching process. The baseline branching rate is a function of time that can be estimated when dendritic data at several developmental time points is available. When data at only one time point is available, what is then the best choice for the baseline branching rate function?
3. A migration rate is assigned to a growth cone at the time of its birth (i.e., after a branching event) by random sampling a given distribution, and remains constant for its life span (i.e., up to its next branching event). Other ways of implementing stochasticity in growth cone migration, however, are also possible (like stochasticity in the actual migration at each time step). Are there other, or even better ways to capture the stochasticity of the underlying biological process, and how to test it?
4. A basic assumption in the model is the independency in branching and migration of growth cones. To what extent do possible correlations in the occurrences of branching and elongation events result in altered variations in dendritic shape parameters?
5. A thorough experimental test of the model is possible when growth cone behavior is quantified in a longitudinal *in vivo* study of identified neurons in development, and the neurons are morphological reconstructed afterwards. What could be the best experimental approach to this end?
6. The power of the growth-model approach is that dendritic geometrical properties and their variations can possibly be captured by a limited set of parameters describing the underlying dendritic growth process. This set of parameters has to be determined for many different neuron types. Such an inventory will give insight in the similarity and dissimilarity of growth actions in the development of different neuron types.

ACKNOWLEDGMENTS

We are very grateful to Dr. M.A. Corner for his critical comments and improvements of the manuscript. Part of this work was supported by NATO grant CRG 930426 (JVP).

REFERENCES

Abbott, L.F. and LeMasson, G. (1993) Analysis of neuron models with dynamically regulated conductances. *Neural Comp*. **5**, 823-842.

Acebes, A. and Ferrus, A. (2000) Cellular and molecular features of axon collaterals and dendrites. *Trends Neurosci*. **23**, 557-565.

Ascoli, G. (2002a) Neuroanatomical algorithms for dendritic modeling. *Network: Computation in Neural Systems* **13**, 247-260.

Ascoli, G. (2002b) Computational Neuroanatomy – Principles and Methods, Edited by G.A. Ascoli. Humana PressTotowa, New Jersey.

Ascoli, G.A., Krichmar, J.L., Scorcioni, R., Nasuto, S.J. and Senft, S.L. (2001) Computer generation and quantitative morphometric analysis of virtual neurons. *Anat. Embryol*. **204**, 283-301.

Bastian, J. and Nguyenkim, J. (2001) Dendritic modulation of burst-like firing in sensory neurons. *J. Neurophysiol*. **85**, 10-22.

Berry, M. and Bradley, P.M. (1976) The application of network analysis to the study of branching patterns of large dendritic fields. *Brain Res*. **109**, 111-132.

Black, M.M. (1994) Microtubule transport and assembly cooperate to generate the microtubule array of growing axons. In *The Self-Organizing Brain: From Growth Cones to Functional Networks*, edited by J. van Pelt, M.A. Corner, H.B.M. Uylings and F.H. Lopes da Silva, Progress in Brain Research, Vol 102, pp. 61-77. Elsevier, Amsterdam.

Burke, R.E., Marks, W.B. and Ulfhake, B. (1992) A parsimonious description of motoneuron dendritic morphology using computer simulation. *J. Neurosc*. **12**, 2403-2416.

Caley, A. (1859) On the analytical forms called trees. *Philos. Mag*. **18**, 374-378.

Cameron, W.E., Averill, D.B. and Berger, A.J. (1985) Quantitative analysis of the dendrites of cat phrenic motoneurons stained intracellularly with horseradish peroxidase *J. Comp. Neurol*. **230**, 91-101.

Carriquiry, A.L., Ireland, W.P., Kliemann, W. and Uemura, E. (1991) Statistical evaluations of dendritic growth models. *Bull. Math. Biol*. **53**, 579-589.

Cline H.T. (1999) Development of dendrites. In: Dendrites, G. Stuart, N. Spruston, M. Hausser (Eds), Oxford Un. Press, 1999, pp35-56.

Costa, L.F., Manoel, E.T.M., Faucereau, F., Chelly, J., Van Pelt, J., and Ramakers, G. (2002) A shape analysis framework for neuromorphomery. *Network: Comput. Neural Syst*. **13**, 283-310.

Cullheim, S., Fleshman, J.W., Glenn, L.L. and Burke, R.E. (1987) Membrane area and dendritic structure in type-identified triceps surae alpha-motoneurons. *J. Comp. Neurol.* **25**, 68-81.

De Ruiter, J.P. and Uylings, H.B.M. (1987) Morphometric and dendritic analysis of fascia dentata granule cells in human aging and senile dementia. *Brain Res*. **402**, 217-229.

Desmond, N.L. and Levy, W.B. (1984) Dendritic caliber and the 3/2 power relationship of dentate granule cells. *J. Comp. Neurol*. **227**, 589-596.

Dityatev, A.E., Chmykhova, N.M., Studer, L., Karamian, O.A., Kozhanov, V.M. and Clamann, H.P. (1995) Comparison of the topology and growth rules of motoneuronal dendrites *J. Comp. Neurol.* **363,** 505-516.

Duijnhouwer, J., Remme, M.W.H., Van Ooyen, A. and Van Pelt, J. (2001) Influence of dendritic morphology on firing patterns in model neurons. *Neurocomputing,* **38-40**, 183-189.

Granato, A. and Van Pelt, J. (2003) Effects of early ethanol exposure on dendrite growth of cortical pyramidal neurons: inferences from a computational model. *Developm. Brain Res*. **142**, 223-227.

Harding, E.F. (1971) The probabilities of rooted tree-shapes generated by random bifurcation. *J. Appl. Prob*. **3**, 44-77.

Hillman, D.E. (1979) Neuronal shape parameters and substructures as a basis of neuronal form. In: *The Neurosciences, 4th Study Program*, edited by F.O. Schmitt and F.G. Worden, pp. 477-498. MIT Press Cambridge.

Hillman, D.E. (1988) Parameters of dendritic shape and substructure: Intrinsic and extrinsic determination? In *Intrinsic Determinants of Neuronal Form and Function*, edited by R.J. Lasek and M.M. Black, pp. 83-113. A.R. Liss, New York.

Horsfield, K., Woldenberg, M.J. and Bowes, C.L. (1987) Sequential and synchronous growth models related to vertex analysis and branching ratios. *Bull. Math. Biol.* **49**, 413-430.

Ireland, W., Heidel, J. and Uemura, E. (1985) A mathematical model for the growth of dendritic trees. *Neurosc. Lett*. **54**, 243-249.

Jaeger, D. (2000) Accurate reconstruction of neuronal morphology. In *Computational Neuroscience: Realistic Modeling for Experimentalists,* edited by E. De Schutter and R.C. Cannon, pp. 159-178. CRC Press, Boca Raton, FL.

Kater, S.B., Davenport, R.W. and Guthrie, P.B. (1994) Filopodia as detectors of environmental cues: signal integration through changes in growth cone calcium levels. In *The Self-Organizing Brain: From Growth Cones to Functional Networks*, edited by J. van Pelt, M.A. Corner, H.B.M. Uylings and F.H. Lopes da Silva, Progress in Brain Research, Vol 102, pp. 49-60. Elsevier, Amsterdam.

Kater, S.B. and Rehder, V. (1995) The sensory-motor role of growth cone filopodia. *Current Opinion in Neurobiology* **5**, 68-74.

Kliemann, W.A. (1987) Stochastic dynamic model for the characterization of the geometrical structure of dendritic processes. *Bull. Math. Biol*. **49**, 135-152.

Koch, C. and Segev, I (1989) *Methods in Neuronal Modeling: From Synapses to Networks*. MIT Press, Cambridge, MA.

Larkman, A.U. (1991) Dendritic morphology of pyramidal neurones of the visual cortex of the rat: I. Branching patterns. *J. Comp. Neurol*. **306**, 307-319.

Larkman, A. and Mason, A. (1990) Correlations between morphology and electrophysiology of pyramidal neurons in slices of rat visual cortex. I. Establishment of cell classes. *J. Neurosc*. **10**, 1407-1414.

Larkman, A.K., Major, G., Stratford, K.J. and Jack, J.J.B. (1992) Dendritic morphology of pyramidal neurones of the visual cortex of the rat. IV: Electrical geometry. *J. Comp. Neurol*. **323**, 137-152.

Letourneau, P.C., Snow, D.M. and Gomez, T.M. (1994) Growth cone motility: substratum-bound molecules, cytoplasmic [Ca^{2+}] and Ca^{2+}-regulated proteins. In *The Self-Organizing Brain: From Growth Cones to Functional Networks*, edited by J. van Pelt, M.A. Corner, H.B.M. Uylings and F.H. Lopes da Silva, Progress in Brain Research, Vol 102, pp. 35-48. Elsevier, Amsterdam.

Mainen, Z.F. and Sejnowski, T.J. (1996) Influence of dendritic structure on firing patterns in model neocortical neurons. *Nature* **382**, 363-366.

Mason, A. and Larkman, A. (1990) Correlations between morphology and electrophysiology of pyramidal neurons in slices of rat visual cortex. II. Electrophysiology. *J. Neurosc*. **10**, 1415-1428.

McAllister, A.K. (2002) Conserved cues for axon and dendritic growth in the developing cortex. Neuron **33**, 2-4.

Nowakowski, R.S., Hayes, N.L. and Egger, M.D. (1992) Competitive interactions during dendritic growth: a simple stochastic growth algorithm. *Brain Research* **576**, 152-156.

Overdijk, J., Uylings, H.B.M., Kuypers, K. and Kamstra, A.W. (1978) An economical, semi-automatic system for measuring cellular tree structures in three dimensions, with special emphasis on Golgi-impregnated neurons. *J. Microsc*. **114**, 271-284.

Poznanski, R.R., Gibson, W.G. and Bennett, M.R. (1995) Electrotonic coupling between 2 CA3 hippocampal pyramidal neurons – A distributed cable model with somatic gap-junction. *Bull. Math. Biol*. **57**, 865-881.

Rall, W. (1959) Branching dendritic trees and motoneuron membrane resistivity. *Exp. Neurol.* **1**, 491-527.

Rall, W., Burke, R., Holmes, W., Jack, J., Redman, S. and Segev, I. (1992) Matching dendritic neuron models to experimental data. *Physiol. Rev.* **72**, 159-186.

Rall, W. (1995) *The theoretical foundation of dendritic function: Selected papers of Wilfrid Rall with commentaries*, edited by I. Segev, J. Rinzel, G.M. Shepherd. MIT Press, Cambridge, MA.

Ramakers, G.J.A., Winter, J., Hoogland, T.M., Lequin, M.B., Van Hulten, P., Van Pelt, J. and Pool, C.W. (1998) Depolarization stimulates lamellipodia formation and axonal but not dendritic branching in cultured rat cerebral cortex neurons. *Dev. Brain Res*. **108**, 205-216.

Ramakers, G.J.A., Avci, B., Van Hulten, P., Van Ooyen, A., Van Pelt, J., Pool, C.W. and Lequin, M.B. (2001) The role of calcium signaling in early axonal and dendritic morphogenesis of rat cerebral cortex neurons under non-stimulated growth conditions. *Dev. Brain Res*. **126**, 163-172.

Ramakers, G.J.A. (2002) Rho proteins, mental retardation and the cellular basis of cognition. *Trends in Neurosciences* **25**, 191-199.

Rapp, M., Segev, I. and Yarom, Y. (1994) Physiology, morphology and detailed passive models of guinea-pig cerebellar Purkinje cells. *J. Physiol*. **474**, 101-118.

Schaefer, A. T., Larkum, M.E., Sakmann, B. and Roth, A. (2003) Coincidence detection in pyramidal neurons is tuned by their dendritic branching pattern. *J. Neurophysiol* . **89**, 3143-3154.

Schierwagen, A. (1986) Segmental cable modelling of electrotonic transfer properties of deep superior colliculus neurons in the cat. *J. Hirnforsch*. **27**, 679-690.

Schierwagen, A. and Grantyn, R. (1986) Quantitative morphological analysis of deep superior colliculus neurons stained intracellularly with HRP in the cat. *J. Hirnforsch*. **27**, 611-623.

Sheasby, B.W. and Fohlmeister, J.F. (1999) Impulse encoding across the dendritic morphologies of retinal ganglion cells. *J. Neurophysiol*. **81**, 1685-1698.

Shreve, R. L. (1966) Statistical law of stream numbers. *J. Geol*. **74**, 17-37.

Smit, G. J., Uylings, H. B. M. and Veldmaat-Wansink, L. (1972) The branching pattern in dendrites of cortical neurons. *Acta Morphol. Neerl.-Scand*. **9**, 253-274.

Song H.J. and Poo, M.M. (2001) The cell biology of neuronal navigation. *Nature Cell Biology* **3**, E81-E88.

Streekstra, G.J. and Van Pelt, J. (2002) Analysis of tubular structures in 3D confocal images. *Network: Comput Neural Syst*. **13**, 381-395.

Tamori, Y. (1993) Theory of dendritic morphology. *Physical Review E* **148**, 3124-3129.

Uemura, E., Carriquiry, A., Kliemann, W. and Goodwin, J. (1995) Mathematical modeling of dendritic growth in vitro. *Brain Research* **671,** 187-194.

Uylings, H.B.M., Kuypers, K., Diamond, M.C. and Veltman, W.A.M. (1978a) Effects of differential environment on plasticity of dendrites of cortical pyramidal neurons in adult rats. *Exp. Neurol.* **62**, 658-677.

Uylings, H.B.M., Kuypers, K. and Veltman, W.A.M. (1978b) Environmental influences on the neocortex in later life. In *Maturation of the nervous system*, edited by M.A. Corner, Progress in Brain Research, Vol 48, pp. 261-273. Elsevier, Amsterdam.

Uylings, H.B.M., Ruiz-Marcos, A. and Van Pelt, J. (1986) The metric analysis of three-dimensional dendritic tree patterns: A methodological review. *J Neurosci Meth.* **18,** 127-151.

Uylings, H.B.M., Van Pelt, J. and Verwer, R.W.H. (1989) Topological analysis of individual neurons. In *Computer Techniques in Neuroanatomy,* edited by J.J. Capowski, pp. 215-239. Plenum, New York.

Uylings, H.B.M., Van Eden, C.G., Parnavelas, J.G. and Kalsbeek, A. (1990) The prenatal and postnatal development of rat cerebral cortex. In *The cerebral cortex of the rat*, edited by B. Kolb and R.C. Tees, pp. 35-76. MIT Press, Cambridge, MA.

Uylings, H.B.M., Van Pelt, J., Parnavelas, J.G. and Ruiz-Marcos, A. (1994) Geometrical and topological characteristics in the dendritic development of cortical pyramidal and non-pyramidal neurons. In *The Self-Organizing Brain: From Growth Cones to Functional Networks*, edited by J. van Pelt, M.A. Corner, H.B.M. Uylings and F.H. Lopes da Silva, Progress in Brain Research, Vol. 102, pp. 109-123. Elsevier, Amsterdam.

Uylings, H.B.M. and Van Pelt, J. (2002) Measures for quantifying dendritic arborizations. *Network: Comput. Neural Syst*. **13**, 397-414.

Van Elburg, R., Fonds, D., and Van Ooyen, A. Influence of dendritic topology on firing patterns in model neurons activated by synaptic stimulation of the dendritic tree (personal communication).

Van Ooyen, A. (1994) Activity-dependent neural network development. *Network: Comput. Neural Syst.* **5** 401-423.

Van Ooyen, A. (2001) Competition in the development of nerve connections: a review of models. *Network: Comput. Neural Syst*. **12**, R1-R47.

Van Ooyen, A. and Willshaw, D.J. (1999) Competition for neurotrophic factor in the development of nerve connections. *Proc. R. Soc. Lond*. B **266**: 883-892.

Van Ooyen, A. and Willshaw, D.J. (2000) Development of nerve connections under the control of neurtrophic factors: parallels with consumer-resource systems in population biology. *J. Theor. Biol*. **206**, 195-210.

Van Ooyen, A. and Van Pelt, J. (2002) Competition in neuronal morphogenesis and the development of nerve connections. In: *Computational Neuroanatomy: Principles and Methods*, edited by G.A. Ascoli, Humana Press Inc. Totowa, NJ, pp. 219-244.

Van Ooyen, A., Duijnhouwer, J., Remme, M.W.H., and Van Pelt, J. (2002) The effect of dendritic topology on firing patterns in model neurons. *Network: Computation in neural systems* **13**, 311-325.

Van Pelt, J. and Verwer, R.W.H. (1983) The exact probabilities of branching patterns under segmental and terminal growth hypotheses. *Bull. Math. Biol.* **45,** 269-285.

Van Pelt, J. and Verwer, R.W.H. (1985) Growth models (including terminal and segmental branching) for topological binary trees. *Bull. Math. Biol.* **47**, 323-336.
Van Pelt, J. and Verwer, R.W.H. (1986) Topological properties of binary trees grown with order-dependent branching probabilities. *Bull. Math. Biol.* **48**, 197-211.
Van Pelt, J., Uylings, H.B.M. and Verwer, R.W.H. (1989) Distributional properties of measures of tree topology. *Acta Stereol.* **8**, 465-470.
Van Pelt, J. (1992) A simple vector implementation of the Laplace-transformed cable equations in passive dendritic trees. *Biol. Cybern.* **68**, 15-21.
Van Pelt, J., Uylings, H.B.M., Verwer, R.W.H., Pentney, R.J. and Woldenberg, M.J. (1992) Tree asymmetry - a sensitive and practical measure for binary topological trees. *Bull. Math. Biol.* **54**, 759-784.
Van Pelt, J. and Schierwagen, A.K. (1994) Electrotonic properties of passive dendritic trees - effect of dendritic topology. In *The Self-Organizing Brain: from Growth Cones to Functional Networks*, edited by J. van Pelt, M.A. Corner, H.B.M. Uylings and F.H. Lopes da Silva, Progress in Brain Research Vol 102, pp. 127-149. Elsevier, Amsterdam .
Van Pelt, J. and Schierwagen, A.K. (1995) Dendritic electrotonic extent and branching pattern topology. In *The Neurobiology of Computation*, edited by J. M. Bower, pp. 153-158. Kluwer, Boston.
Van Pelt, J. (1997) Effect of pruning on dendritic tree topology *J. Theor. Biol*. **186**, 17-32.
Van Pelt, J., Dityatev, A.E. and Uylings, H.B.M. (1997) Natural variability in the number of dendritic segments: model-based inferences about branching during neurite outgrowth. *J. Comp. Neurol*. **387**, 325-340.
Van Pelt, J. and Uylings, H.B.M. (1999) Modeling the natural variability in the shape of dendritic trees: application to basal dendrites of small rat cortical layer 5 pyramidal neurons. *Neurocomputing* **26-27**, 305-311.
Van Pelt, J., Schierwagen, A., and Uylings, H.B.M. (2001a) Modeling dendritic morphological complexity of deep layer cat superior colliculus neurons. *Neurocomputing* **38-40,** 403-408.
Van Pelt J, Van Ooyen A and Uylings H.B.M. (2001b) Modeling dendritic geometry and the development of nerve connections. In *Computational Neuroscience, realistic modeling for experimentalists*, edited by E. de Schutter and R.C. Cannon, pp. 179-208. Boca Raton, CRC Press.
Van Pelt, J., Van Ooyen, A., and Uylings, H.B.M. (2001c) The need for integrating neuronal morphology databases and computational environments in exploring neuronal structure and function. *Anat Embryol*. **204**, 255-265.
Van Pelt, J. and Uylings, H.B.M. (2002) Branching rates and growth functions in the outgrowth of dendritic branching patterns. *Network: Comput. Neural Syst*. **13**, 261-281.
Van Pelt, J. (2002) Special issue on quantitative neuroanatomy and neuroinformatics. *Network: Comput. Neural Syst.* ***13***.
Van Pelt, J. and Uylings, H.B.M. (2003) Growth functions in dendritic outgrowth. *Brain and Mind* **4**, 51-65.
Van Pelt, J., Graham, B.P. and Uylings, H.B.M. (2003) Formation of dendritic branching patterns. In *Modeling Neural Development* , edited by A. van Ooyen, pp 75-94. MIT Press, Cambridge, MA.
Van Veen, M.P. and Van Pelt, J. (1993) Terminal and intermediate segment lengths in neuronal trees with finite length. *Bull. Math. Biol*. **55**, 277-294.
Verwer, R.W.H., Van Pelt, J., and Uylings, H.B.M. (1992) An introduction to topological analysis of neurones. In *Quantitative Methods in Neuroanatomy*, edited by M.G. Stewart, pp. 295-323. John Wiley & Sons.
Vetter, P., Roth, A. and Hausser, M. (2001) Propagation of action potentials in dendrites depends on dendritic morphology. J. Neurophysiol. **85**, 926-937.
Washington, S.D., Ascoli, G.A. and Krichmar, J.L. (2000) A statistical analysis of dendritic morphology's effect on neuron electrophysiology of CA3 pyramidal cells. *Neurocomputing* **32-33**, 261-269.
Whitford, K.L., Marillat, V., Stein, E.W., Goodman, C.S., Tessier-Lavigne, M., Chedotal, A. and Ghosh, A. (2002) Regulation of cortical dendrite development by slit-robo interactions. *Neuron* **33**: 47-61.
Woldenberg, M.J., O'Neill, M.P., Quackenbush, L.J. and Pentney, R.J. (1993) Models for growth, decline and regrowth of the dendrites of rat Purkinje cells induced from magnitude and link-length analysis. *J. Theor. Biol*. **162**, 403-429.
Zhang, L.I. and Poo, M.M. (2001) Electrical activity and development of neural circuits. *Nature Neurosci.* **4** Suppl, 1207-14.